Chapter

Supercritical-Fluids Thermophysical Properties and Heat Transfer in Power-Engineering Applications

Igor L. Pioro

Abstract

Researches on specifics of thermophysical properties and heat transfer at supercritical pressures (SCPs) started as early as the 1930s with the study on free-convection heat transfer to fluids at a near-critical point. In the 1950s, the concept of using SC "steam" to increase thermal efficiency of coal-fired thermal power plants became an attractive option. Germany, USA, the former USSR, and some other countries extensively studied heat transfer to SC fluids (SCFs) during the 1950s till the 1980s. This research was primarily focused on bare circular tubes cooled with SC water (SCW). However, some studies were performed with modeling fluids such as SC carbon dioxide and refrigerants instead of SCW. Currently, the use of SC "steam" in coal-fired thermal power plants is the largest industrial application of fluids at SCPs. Near the end of the 1950s and at the beginning of the 1960s, several studies were conducted to investigate a possibility of using SCW as a coolant in nuclear reactors with the objective to increase thermal efficiency of nuclear power plants (NPPs) equipped with water-cooled reactors. However, these research activities were abandoned for some time and regained momentum in the 1990s. In support of the development of SCW-cooled nuclear-power reactor (SCWR) concepts, first experiments have been started in annular and various bundle flow geometries. At the same time, more numerical and CFD studies have been performed in support of our limited knowledge on specifics of heat transfer at SCPs in various flow geometries. As the first step in this process, heat transfer to SCW in vertical bare tubes can be investigated as a conservative approach (in general, heat transfer in fuel bundles will be enhanced with various types of appendages, that is, grids, end plates, spacers, bearing pads, fins, ribs, etc.). New experiments in the 1990–2000s were triggered by several reasons: (1) thermophysical properties of SCW and other SCFs have been updated from the 1950s–1970s, for example, a peak in thermal conductivity in the critical/pseudocritical points was "officially" introduced in 1990s; (2) experimental techniques have been improved; (3) in SCWRs, various bundle flow geometries will be used instead of bare-tube geometry; (4) in SC "steam" generators of thermal power plants, larger diameter tubes/pipes (20–40 mm) are used, however in SCWRs hydraulic-equivalent diameters of proposed bundles will be within 5–12 mm; (5) with Research and Development (R&D) of next-generation or Generation-IV nuclear-power-reactor concepts, new areas of application for SCFs have appeared—for example, SCP helium was proposed to be used as a reactor coolant, SCP Brayton

and Rankine cycles with SC carbon dioxide as a working fluid are being developed, etc. A comparison of thermophysical properties of SCFs with those of subcritical-pressure fluids showed that SCFs as single-phase fluids have unique properties, which are close to "liquid-like" behavior below critical or pseudocritical points and are quite similar to the behavior of "gas-like" substances above these points. A comparison of selected SCW heat transfer correlations has shown that their results may differ from one to another by more than 200%. Based on these comparisons, it became evident that there is a need for reliable, accurate, and wide-range SCW heat transfer correlation(s) to be developed and verified. Therefore, the objective of this chapter is to summarize in concise form specifics of supercritical-fluids thermophysical properties and heat transfer in power-engineering applications.

Keywords: supercritical water, carbon dioxide, refrigerant, forced convective heat transfer

1. Introduction

1.1 Historical note on using supercritical fluids (SCFs)

The use of supercritical fluids (SCFs) in various processes is not new and, actually, is not a human invention. Nature has been processing minerals in aqueous solutions at near or above the critical point of water for billions of years. In the late 1800s, scientists started to use this natural process in their labs for creating various crystals. During the last 50–60 years, this process, called hydrothermal processing (operating parameters: water pressure from 20 to 200 MPa and temperatures from 300 to 500°C), has been widely used in the industrial production of high-quality single crystals (mainly gem stones) such as sapphire, tourmaline, quartz, titanium oxide, zircon and others [1].

Also, compressed water, that is, water at a supercritical pressure (SCP), but at a temperature below $T_{cr} \approx 374$°C, exists in oceans at the depth of ~2.2 km and deeper. If at this depth there is an active underwater volcano with the temperature of a magma above T_{cr} of water, conditions for existence of supercritical water (SCW) can be reached.

The first works devoted to the problem of heat transfer at supercritical pressures (SCPs) started as early as the 1930s. Schmidt et al. [2] investigated free-convection heat transfer to fluids at a near-critical point with the application to a new effective cooling system for turbine blades in jet engines. They found that the free-convection heat transfer coefficient (HTC) at the near-critical state was quite high, and decided to use this advantage in single-phase thermosyphons with an intermediate working fluid at the near-critical point [3].

In the 1950s, the idea of using SC "steam" (actually, SCW) appeared to be rather attractive for the Rankine power cycle. The objective was to increase a thermal efficiency of coal-fired thermal power plants (ThPPs) (see **Table 1**). This change, that is, substantially higher operating pressures in the Rankine cycle from subcritical ones, and, correspondingly to that, higher inlet-turbine temperature up to 625°C, has allowed increasing of thermal efficiencies from 40–43% to 50–55% (gross) (in total by 7–15%). Currently, SCP coal-fired thermal power plants (world electricity generation with coal 38%—the largest source for electricity generation; in India—77%; China—65%; Germany—37%; and in USA—30%) are the second ones by thermal efficiencies after gas-fired combined-cycle ThPPs (world electricity generation with natural gas 23%—second largest source for electricity generation; in

No.	Power plant	Gross thermal efficiency
1	Combined-cycle ThPP (combination of Brayton gas-turbine cycle (fuel—natural gas or LNG); combustion-products parameters at gas turbine: $P_{in} \approx 2.3$ MPa and $T_{in} \approx 1650$°C) and Rankine cycle steam-turbine parameters: $P_{in} \approx 12.5$ MPa and $T_{in} \approx 585$°C ($T_{cr} = 374$°C)	Up to 62%
2	SCP coal-fired ThPP (Rankine cycle "steam"-turbine parameters (see **Figure 1**): $P_{in} \approx 23.5$–38 MPa ($P_{cr} = 22.064$ MPa), $T_{in} \approx 540$-625°C ($T_{cr} = 374$°C) and steam reheat at: $P \approx 0.25 \cdot P_{in}$ and $T_{reheat} \approx 540$-625°C)	Up to 55%
3	Subcritical-pressure coal-fired ThPP (older plants; Rankine cycle steam-turbine parameters (see **Figure 2**): $P_{in} = 17$ MPa ($T_{sat} = 352$°C), $T_{in} = 540$°C ($T_{cr} = 374$°C), and steam reheat at: $P \approx 0.25 \cdot P_{in}$ and $T_{reheat} = 540$°C)	Up to 43%
4	Carbon dioxide-cooled reactor (advanced gas-cooled reactor (AGR)) NPP (Generation-III) (reactor coolant (carbon dioxide): $P = 4$ MPa and $T = 290$–650°C; Rankine cycle steam-turbine parameters (see **Figure 2**): $P = 17$ MPa ($T_{sat} = 352$°C); $T_{in} = 540$°C ($T_{cr} = 374$°C), and steam reheat at: $P \approx 0.25 \cdot P_{in}$ and $T_{in} = 540$°C)	Up to 42%
5	Sodium-cooled fast reactor (SFR) (BN-600; BN-800) NPP (reactor coolant (sodium): $P \approx 0.1$ MPa (above sodium level) and $T_{max} = 550$°C; Rankine cycle steam-turbine parameters (see **Figure 3**): $P = 14$ MPa ($T_{sat} = 337$°C); $T_{in} = 505$°C ($T_{cr} = 374$°C) and steam reheat at: $P \approx 0.25 \cdot P_{in}$ and $T_{in} = 505$°C)	Up to 40%
6	Pressurized water reactor (PWR) NPP (Generation-III+, new reactors) (reactor coolant (light water): $P = 15.5$ MPa ($T_{sat} = 345$°C) and $T = 280$-322°C; Rankine cycle steam-turbine parameters (see **Figure 4**): $P = 7.8$ MPa and $T_{in} = T_{sat} = 293$°C and steam reheat at $P_{in} \approx 1$ MPa and $T_{in} \approx 273$°C)	Up to 36-38%
7	Pressurized water reactor (PWR) NPP (Generation-III, current fleet) (reactor coolant: $P = 15.5$ MPa ($T_{sat} = 345$°C) and $T = 292$–329°C; Rankine cycle steam-turbine parameters (see **Figure 4**): $P = 6.9$ MPa and $T_{in} = T_{sat} = 285$°C and steam reheat at $P_{in} \approx 1$ MPa and $T_{in} \approx 265$°C)	Up to 34-36%
8	Boiling-water-reactor (BWR) or advanced BWR NPP (Generation-III and III+, current fleet) ($P_{in} = 7.2$ MPa and $T_{in} = T_{sat}$=288°C (direct cycle) and steam reheat at $P_{in} \approx 1$ MPa and $T_{in} \approx 268$°C (see **Figure 4**))	Up to 34%
9	Pressurized heavy water reactor (PHWR) NPP (Generation-III, current fleet) (reactor coolant: $P_{out} = 10$ MPa ($T_{sat} = 311$°C) and $T = 260$–310°C; Rankine cycle steam-turbine parameters: $P = 4.6$ MPa and $T_{in} = T_{sat} = 259$°C and steam reheat at l $P_{in} \approx 1$ MPa and $T_{in} \approx 240$°C)	Up to 32%

Table 1.
Typical ranges of thermal efficiencies (gross) of modern thermal and nuclear power plants (NPPs) [4, 5] (for details including schematics and T-s diagrams, see Handbook [6] and Dragunov et al. [7]).

Russia—59%; UK—44%; Italy—42%; and in USA—34%) [4, 5]. More details on ThPPs can be found in Pioro and Kirillov [8] and many other sources.

Also, at SCPs there is no liquid-vapor-phase transition; therefore, there is no such phenomenon as critical heat flux (CHF) or dryout. It is only within a certain range of parameters a deteriorated heat transfer (DHT) regime may occur. Work in this area was mainly performed in Germany, USA, former USSR, and some other countries in the 1950–1980s [9].

1.2 Future applications of SCFs in next-generation nuclear-power reactors and NPPs

At the end of the 1950s and the beginning of the 1960s, early studies were conducted to investigate a possibility of using SCW in nuclear reactors. Several concepts of nuclear reactors using SCW were developed in Great Britain, France,

USA, and former USSR. However, this idea was abandoned for almost 30 years with the emergence of light water reactors (LWRs), but regained interest in the 1990s following LWRs maturation ([6, 9–13]).

This interest was triggered by economical considerations, because nuclear power plants (NPPs) with LWRs (and, especially, with PHWRs) have relatively low thermal efficiencies within the range of 30–36% for Generation-III reactors and up to 37% (38%) for advanced reactors of Generation-III+ (see **Table 1**) compared to those of modern ThPPs (up to 62% for combined-cycle plants and up to 55% for SCP Rankine cycle plants (see **Table 1**)) [6]. Therefore, NPPs with various designs of water-cooled reactors at subcritical pressures cannot compete with modern advanced ThPPs. Also, it should be noted that currently, water-cooled reactors are the vast majority of nuclear-power reactors in the world [14, 15]: (1) PWRs—

No.	Nuclear power plant	Gross eff., %
1	Very high-temperature reactor (VHTR) NPP (reactor coolant—helium (SCF): P = 7 MPa and T_{in}/T_{out} = 640/1000°C; primary power cycle—direct SCP Brayton helium-gas-turbine cycle; possible back-up—indirect Brayton or combined cycles (see **Figures 5** and **6**))	≥55
2	Gas-cooled fast reactor (GFR) or high-temperature reactor (HTR) NPP (reactor coolant—helium (SCF): P = 9 MPa and T_{in}/T_{out} = 490/850°C; primary power cycle—direct SCP Brayton helium-gas-turbine cycle (see **Figure 7**); possible back-up—indirect SCP Brayton or combined cycles (see **Figures 8** and **9**))	≥50
3	Supercritical water-cooled reactor (SCWR) NPP (one of Canadian concepts; reactor coolant—SC light water: P = 25 MPa and T_{in}/T_{out} = 350/625°C (T_{cr} = 374°C); direct cycle; SCP Rankine cycle with high-temperature secondary-steam superheat: T_{out} = 625°C; possible back-up–indirect SCP Rankine "steam"-turbine cycle with high-temperature secondary-steam superheat) (for details of SCP Rankine cycle, see **Table 1** Item No. 2 and **Figure 1**)	45–50
4	Molten salt reactor (MSR) NPP (reactor coolant—sodium-fluoride salt with dissolved uranium fuel: T_{in}/T_{out} = 700/800°C; primary power cycle—indirect SCP carbon dioxide Brayton gas-turbine cycle; possible back-up—indirect Rankine steam-turbine cycle)	~50
5	Lead-cooled fast reactor (LFR) NPP (Russian design BREST-OD-300*: reactor coolant—liquid lead: $P \approx 0.1$ MPa and T_{in}/T_{out} = 420/540°C; primary power cycle—indirect subcritical-pressure Rankine steam cycle: $P_{in} \approx 17$ MPa (P_{cr} = 22.064 MPa) and T_{in}/T_{out} = 340/505°C (T_{cr} = 374°C); high-temperature secondary-steam superheat (in one of the previous designs of BREST-300 NPP primary power cycle was indirect SCP Rankine "steam" cycle: $P_{in} \approx 24.5$ MPa (P_{cr} = 22.064 MPa) and T_{in}/T_{out} = 340/520°C (T_{cr} = 374°C); also, note that power-conversion cycle in a different LFR designs from other countries is based on SCP carbon dioxide Brayton gas-turbine cycle	~41–43
6	Sodium-cooled fast reactor (SFR) NPP (Russian design BN-600: reactor coolant—liquid sodium (primary circuit): $P \approx 0.1$ MPa and T_{in}/T_{out} = 380/550°C; liquid sodium (secondary circuit): T_{in}/T_{out} = 320/520°C; primary power cycle—indirect Rankine steam-turbine cycle: $P_{in} \approx 14.2$ MPa ($T_{sat} \approx 337$°C) and $T_{in\ max}$ = 505°C (T_{cr} = 374°C); secondary-steam superheat: $P \approx 2.45$ MPa and T_{in}/T_{out} = 246/505°C; possible back-up in some other countries—indirect SCP carbon dioxide Brayton gas-turbine cycle)	~40

**BREST-OD-300 is Fast Reactor with "NATural safety"-Test-Demonstration in Russian abbreviations (БРЕСТ-OD-300—Быстрый Реактор с ЕСТественной безопасностью—Опытно –Демонстрационный).*

Table 2.
Estimated ranges of thermal efficiencies (gross) of Generation-IV NPP concepts (Generation-IV concepts are listed according to thermal-efficiency decrease) [6, 16].

299 units or 68% from the total number of 441 units; (2) BWRs—65 units or 15%; (3) PHWRs—48 units or 11%; (4) light water, graphite-moderated reactors (LGRs)—13 units of 3%.

Therefore, six concepts of nuclear-power reactors/NPPs of next generation, Generation-IV, were proposed (see **Table 2**), which will have thermal efficiencies comparable with those of modern thermal power plants. Supercritical water-cooled reactor (SCWR) is one of these six concepts under development in a number of countries [6, 17]. Analysis of Generation-IV concepts listed in **Table 2** shows that SCFs, such as helium and water, will be used as reactor coolants, and SCFs such as helium, nitrogen (or mixture of nitrogen (80%) and helium (20%)), carbon dioxide, and water will be used as working fluids (WFs) in power Brayton and Rankine cycles (critical parameters of selected SCFs are listed in **Table 3**). However, it should be mentioned that helium as the reactor coolant and as the working fluid in Brayton power cycle will be at supercritical conditions, which are far above by pressure and temperature critical parameters, that is, helium will behave as compressed gas.

Nowadays, the most widely used SCFs are water, carbon dioxide, and refrigerants [9]. Quite often, carbon dioxide and refrigerants are considered as modeling fluids and used instead of SCW due to significantly lower critical pressures and temperatures, which decreases the complexity and costs of thermalhydraulic experiments. However, they can be/will be used as working fluids in new SCP power cycles: Brayton and Rankine ones [6] (for details, see **Table 3**).

Also, other applications of SCFs will be discussed in the following chapters and are listed in Pioro and Duffey [9].

No.	Fluid	Molar mass	T_{cr}	P_{cr}	ρ_{cr}	Application in power engineering at SCPs
		kg/kmol	°C	MPa	kg/m^3	
1	Carbon dioxide,[1] CO_2	44.01	30.978	7.3773	467.6	WF in Brayton and Rankine power cycles (see **Figures 5** and **6**)
2	Ethanol, C_2H_6O	46.068	241.56	6.268	273.19	N/A
3	Helium,[2] He	4.0026				Reactor coolant in VHTR & GFR (see **Figure 7**); WF in Brayton power cycle (see **Figure 7**)
4	Methanol, CH_3OH	32.042	239.45	8.1035	275.56	N/A
5	Nitrogen, N_2	28.013	-146.96	3.3958	313.3	WF in Brayton cycle (also, mixture of N_2 (80%) & He (20%) is proposed (see **Figures 8** and **9**))
6	R-12, CCl_2F_2	120.91	111.97	4.1361	565.0	Modeling fluid in thermalhydraulic tests
7	R-134a, CF_3CH_2F	102.03	101.06	4.0593	511.9	Modeling fluid in thermalhydraulic tests
8	Water[3], H_2O	18.015	373.95	22.064	322.0	WF in Rankine cycle of coal-fired ThPP; reactor coolant in SCWR; WF in Rankine power cycle (see **Figure 1**)

[1,2,3]*Thermodynamics diagrams: P-T and T-s can be found in Handbook [6].*
[3]*Thermodynamics diagrams: P-T and T-s are shown in* **Figure 10**.

Table 3.
Critical parameters of selected fluids and gases (based on NIST [25]).

2. Specifics of thermophysical properties of SCFs

Prior to a general discussion on specifics of forced-convective heat transfer at critical and supercritical pressures, it is important to define special terms and expressions used at these conditions [6, 9]. For a better understanding of these

No.	Literature source	Fluid	P, MPa	T, °C	Properties
1	Pioro et al. [19]	Properties of selected metals, alloys, and diamond Properties of selected insulating materials Radiative properties of selected materials Properties of selected nuclear fuels Properties of selected gases at atmospheric pressure Properties of selected cryogenic gases Properties of selected fluids on saturation line Properties of selected supercritical fluids Properties of selected liquid alkali metals Thermophysical properties of nuclear-reactor coolants			
2	Handbook [6]	H_2O, CO_2, He	-	-	T-s diagrams
		H_2O (BWR, PHWR, PWR)	7, 11, 15	50-375	ρ, k, μ, ν, c_p, H, **Pr**, β
		H_2O (SCW)	P_{cr}, 25, 30, 35, 40	350-600	ρ, k, μ, ν, c_p, H, **Pr**, β
		CO_2 (SC CO_2)	P_{cr}, 8.4, 10.0, 11.7	0-165	ρ, k, μ, ν, c_p, H, **Pr**, β
		He	P_{cr} and other pressures	Range of T	k, c_p, β
		Air, Ar, CO_2, He, H_2, Kr (gases)	0.1	0-1000	ρ, k, μ, c_p, **Pr**, β
		CO_2 (AGR)	4	250-1000	ρ, k, μ, c_p, H, **Pr**, β
		FLiNaK (MSR)	0.1		
		H_2O/SCW (PWR/SCWR)	15.5/25		
		He (VHTR, GFR)	7, 9		
		Na, Pb, Pb-Bi (SFR, LFR)	0.1		
3	Mann and Pioro [20]	SC R-134a	P_{cr}, 5, 10, 13, 15	-100-175	k, c_p, β
4	Gupta et al. [21]	SCW SC CO_2 SC R-134a (three fluids on same graph)	25.0 8.4* 4.6*	$(0.5-1.6)\frac{T}{T_{cr}}$	ρ, k, μ, c_p, H, **Pr**
5	Pioro and Mokry [22]	H_2O	-	-	T-s diagram
		H_2O (SCW)	P_{cr}, 25, 30, 35	350-600	ρ, k, μ, ν, c_p, H, **Pr**, β
		R-12 (SC R-12)	P_{cr}, 4.65	0-350	ρ, k, μ, ν, c_p, H, **Pr**, β
6	Pioro and Duffey [9]	R-134a (SC R-134a)	P_{cr}, 4.6	70-150	ρ, k, μ, ν, c_p, H, **Pr**, β

**Pressures for SC carbon dioxide, R-134a, and R-12 are equivalent for SCW pressure of 25 MPa, based on, so-called, reduced-pressure scaling:* $\left(\frac{P}{P_{cr}}\right)_{Fluid} = \left(\frac{P}{P_{cr}}\right)_{SCW}$.

Table 4.
Selected list of literature sources on thermophysical properties of fluids, gases, and other materials.

terms and expressions their definitions are listed in Glossary (see below) (also, see **Figures 10**–**35**). Specifics of thermophysical properties at SCPs are described in Pioro et al. [23]; Handbook [6]; Mann and Pioro [24]; Gupta et al. [25]; Pioro and Mokry [26]; and Pioro and Duffey [9] (for more details, see **Table 4**).

Glossary

Compressed fluid is the fluid at a pressure above the critical pressure, but at a temperature below the critical temperature (see **Figure 10**).

Critical point (also called a critical state) is the point in which the distinction between the liquid and gas (or vapor) phases disappears (see **Figure 10**), that is, both phases have the same temperature, pressure, and specific volume or density. The critical point is characterized with the phase-state parameters: T_{cr}, P_{cr} and v_{cr} (or ρ_{cr}), which have unique values for each pure substance.

Deteriorated heat transfer (DHT) is characterized with lower values of the HTC compared to those for normal heat transfer (NHT); and hence, has higher values of wall temperature within some part of a heated channel (see **Figures 12, 13a, 24b, 25b, 27, 31**, and **35**) or within the entire heated length (see **Figure 14b**).

Improved heat transfer (IHT) is characterized with higher values of the HTC compared to those for NHT; and hence, lower values of wall temperature within some part of a heated channel (see **Figures 12, 21, 25, 27b, 33**, and **34**) or within the entire heated length. In our opinion, the IHT regime or mode includes peaks or "humps" in the HTC profile near the critical or pseudocritical points.

Normal heat transfer (NHT) can be characterized in general with HTCs similar to those of subcritical convective heat transfer far from the critical or pseudocritical regions, when they are calculated according to the conventional single-phase Dittus-Boelter-type correlations: $\mathbf{Nu} = 0.0243\ \mathbf{Re}^{0.8}\mathbf{Pr}^{0.4}$ (see **Figures 12, 13a, 14a, 21, 24, 25, 27**, and **30**–**34**).

Overheated vapor is the vapor at pressures below the critical pressure, and at temperatures above the saturation temperature, but below the critical temperature (see **Figure 10**).

Pseudocritical line is the line, which consists of pseudocritical points (see **Figure 10**).

Pseudo-boiling is a physical phenomenon similar to subcritical-pressure nucleate boiling, which may appear at SCPs. Due to heating of an SCF with a bulk-fluid temperature below the pseudocritical temperature (high-density fluid, i.e., "liquid-like") (see **Figures 10, 11, 13b** and **15**), some layers near the heated surface may attain temperatures above the pseudocritical temperature (low-density fluid, i.e., "gas-like"). This low-density "gas-like" fluid leaves the heated surface in a form of variable density volumes (bubbles). During the pseudo-boiling, the HTC usually increases (IHT regime).

Pseudocritical point (characterized with P and T_{pc}) is the point at a pressure above the critical pressure and at a temperature ($T_{pc} > T_{cr}$) corresponding to the maximum value of specific heat at this particular pressure (see **Figures 10, 11**, and **13b**).

Pseudo-film boiling is a physical phenomenon similar to subcritical-pressure film boiling, which may appear at SCPs. At pseudo-film boiling, a low-density fluid (a fluid at temperatures above the pseudocritical temperature, i.e., "gas-like") prevents a high-density fluid (a fluid at temperatures below the pseudocritical temperature, i.e., "liquid-like") from contacting ("rewetting") a heated surface. Pseudo-film boiling leads to the DHT regime.

Supercritical fluid is the fluid at pressures and temperatures that are higher than the critical pressure and critical temperature (see **Figure 10**). However, in the

present paper, the term *supercritical fluid* usually includes both terms—*supercritical fluid* and *compressed fluid*.

Supercritical "steam" is actually supercritical water, because at supercritical pressures fluid is considered as a single-phase substance (see **Figure 10**). However, this term is widely (and incorrectly) used in the literature in relation to supercritical-"steam" generators and turbines.

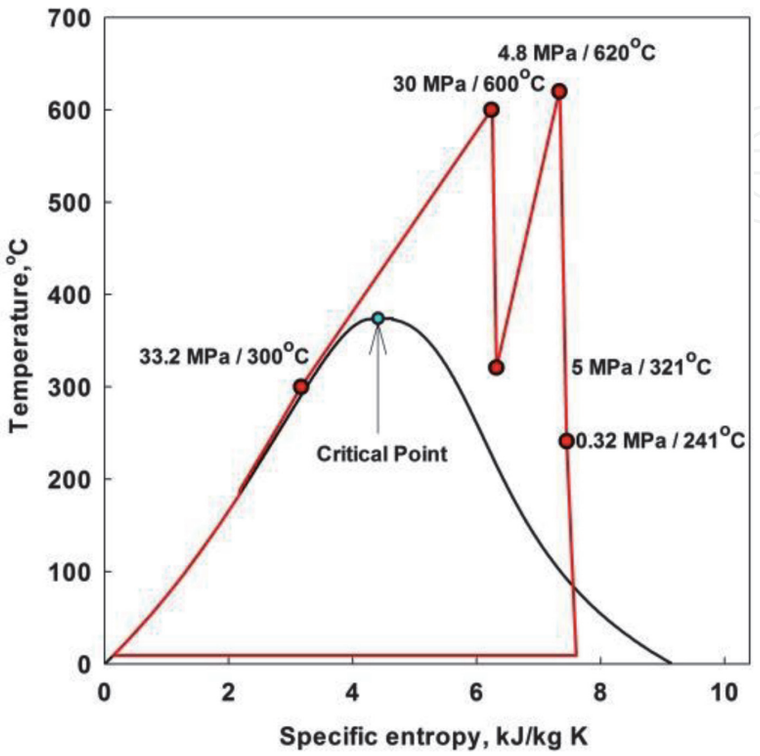

Figure 1.
T-s diagram of generic SCP Rankine "steam"-turbine power cycle (modern advanced coal-fired thermal power plants and future SCWR NPPs) [6, 7].

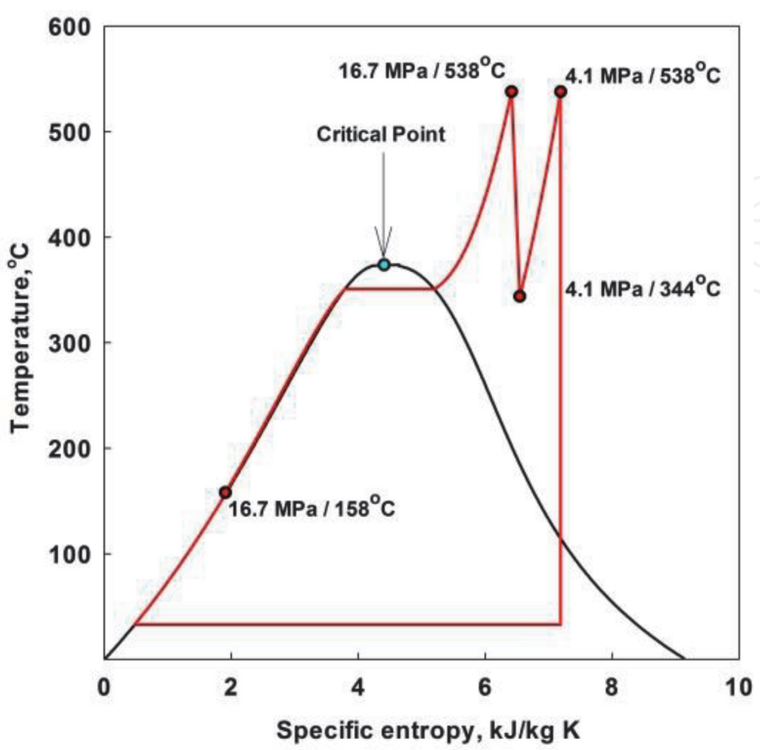

Figure 2.
T-s diagram of generic subcritical-pressure Rankine steam-turbine power cycle (older coal-fired thermal power plants and AGR Torness NPP) [6, 7].

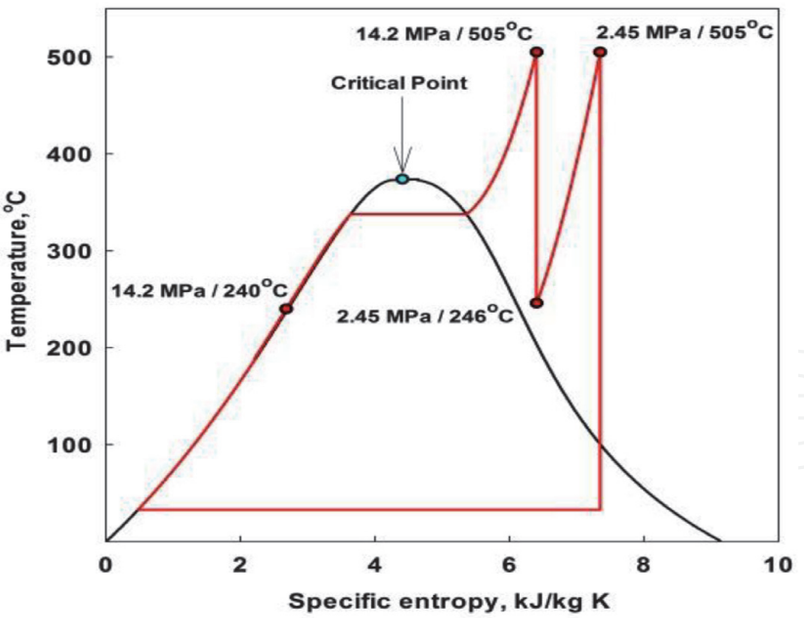

Figure 3.
T-s diagram of generic subcritical-pressure Rankine steam-turbine power cycle (old coal-fired thermal power plants and SFR NPPs) [6, 7].

Superheated steam is the steam at pressures below the critical pressure, but at temperatures above the critical temperature (see **Figure 10**).

Also, profiles of the basic thermophysical properties (density, thermal conductivity, dynamic viscosity, specific heat and specific enthalpy) and Prandtl number for four SCFs: water, ethanol, methanol, and carbon dioxide; at critical and one supercritical pressure, which is 25 MPa for water and the corresponding to that equivalent pressures for all other SCFs vs. reduced temperature (temperature) are shown in **Figures 15–20**.

3. Specifics of forced-convection heat transfer at supercritical pressures

3.1 Vertical bare tubes

Water is the most widely used coolant or working fluid at SCPs. The largest application of SCW is in SC "steam" generators and turbines, which are widely used in the thermal power industry worldwide. Currently, upper limits of pressures and temperatures used in the thermal-power industry are about 30–38 MPa and 600–625°C, respectively (see **Table 1**). A new direction in SCW application in the power industry has been the development of SCWR concepts (see **Table 2**), as part of the Generation-IV International Forum (GIF) [27] initiative (for details, see [6, 9–13, 28–30]; and Proceedings of the International Symposiums on SCWRs (ISSCWR) (selected augmented and revised papers from ISSCWRs have been published in the ASME Journal of Nuclear Engineering and Radiation Science in 2020, Vol. 6 No. 3; in 2018, Vol. 4, No. 1, and 2016, Vol. 2, No. 1).

Experiments at SCPs are very expensive and require sophisticated equipment and measuring techniques. Therefore, some of these studies (e.g., heat transfer in fuel-bundle simulators) are proprietary and, hence, usually are not published in open literature.

The majority of studies deal with heat transfer and hydraulic resistance of working fluids, mainly water, carbon dioxide, refrigerants, and helium, in circular bare tubes [9, 22, 31–34]. A limited number of studies were devoted to heat transfer and pressure drop in annuli and bundles [9, 10, 35–45].

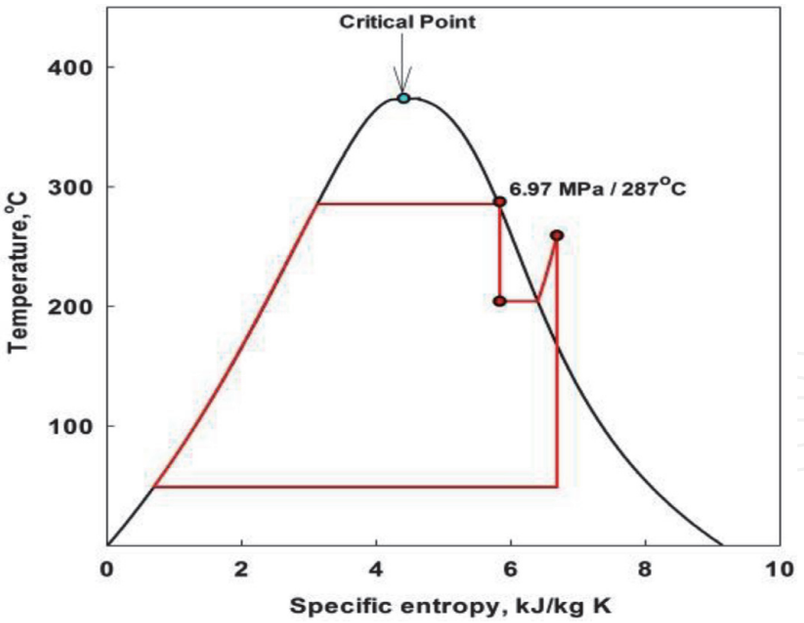

Figure 4.
T-s diagram of generic subcritical-pressure Rankine saturated-steam-turbine power cycle (PWR and BWR NPPs) [6, 7].

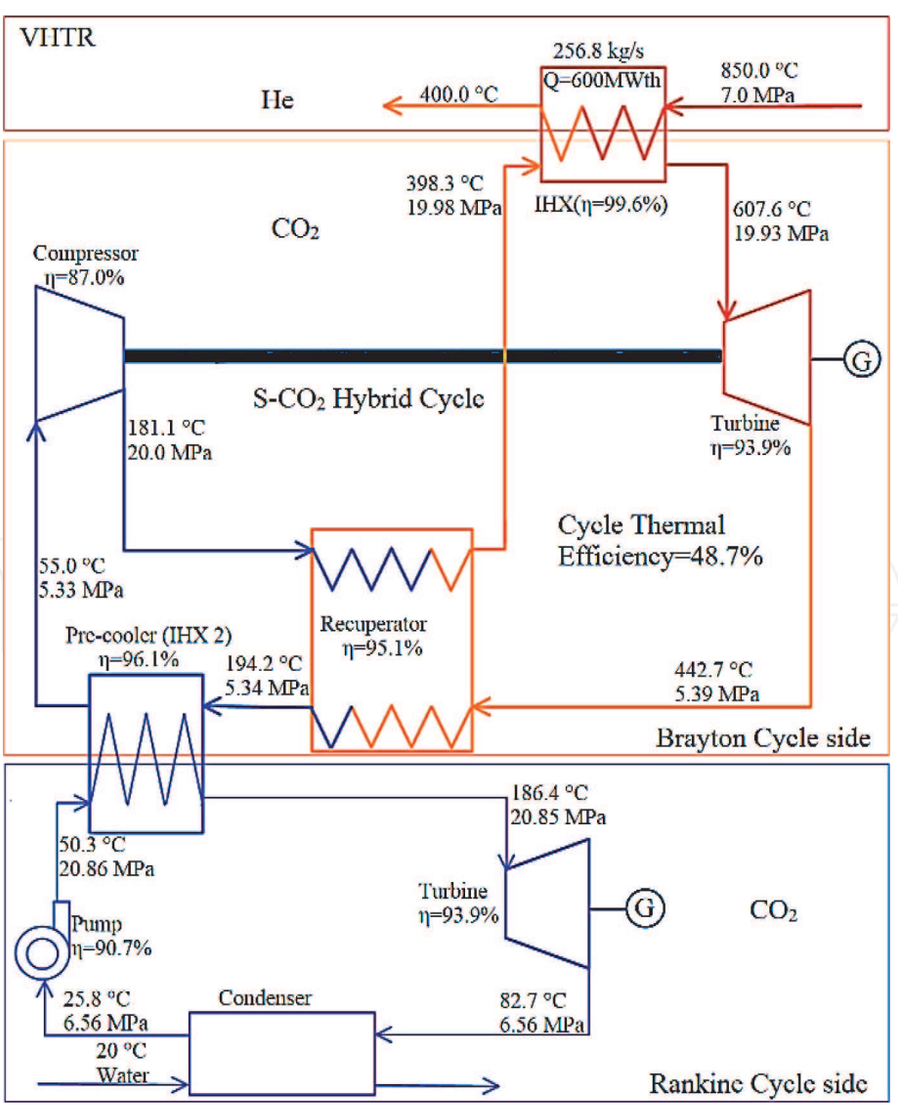

Figure 5.
Layout of 600-MW_{th} VHTR NPP with SC-CO_2 power cycle (based on figure from Bae et al. [17]) [18].

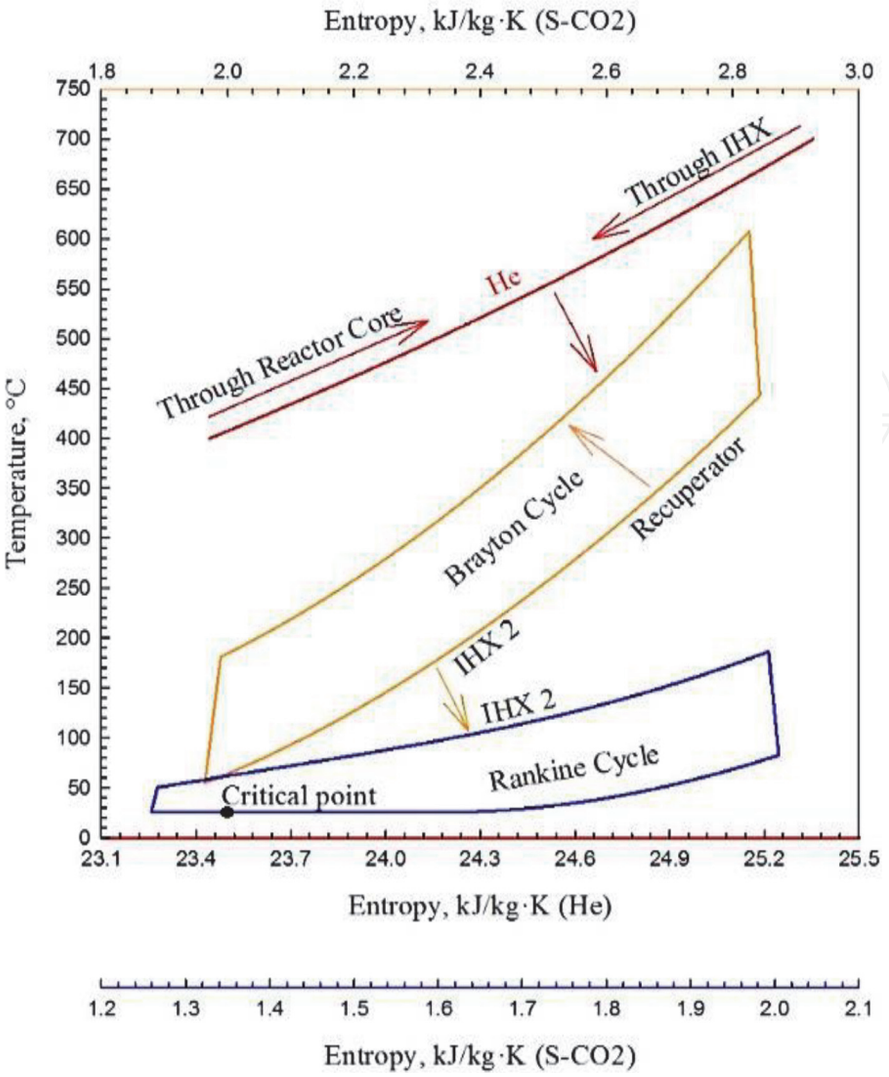

Figure 6.
T-s diagram for 600-MW_{th} VHTR NPP with SC-CO_2 (S-CO_2) power cycle (based on **Figure 5***) [18].*

New experiments in the 1990s–2000s were triggered by several reasons: (1) thermophysical properties of SCW have been updated from the 1950s–1970s, for example, a peak in thermal conductivity in the critical/pseudocritical points was "officially" introduced in the 1990s; (2) experimental techniques have been improved; (3) in SCWRs various bundle flow geometries will be used instead of bare-tube geometry; and (4) in SC "steam" generators of thermal power plants larger diameter tubes/pipes (20–40 mm) are used, however, in SCWRs hydraulic-equivalent diameters of proposed bundles will be within 5–12 mm.

Accounting that SCW, SC carbon dioxide and SC R-12 are the most widely used fluids, specifics of heat transfer, including generalized correlations, will be discussed in this paper. Specifics of heat transfer and pressure drop at other conditions and/or for other fluids are discussed in the book by Pioro and Duffey [9].

All primary sources (i.e., all sources found by the authors from a total of 650 references dated mainly from 1950 till beginning of 2006) of heat transfer experimental data for water and carbon dioxide flowing inside circular tubes at supercritical pressures are listed in the book by Pioro and Duffey [9].

In general, three major heat transfer regimes (for their definitions, see Section 2, Glossary) can be noticed at critical and supercritical pressures (for details, see **Figures 12, 13a, 14, 21, 24, 25, 27, 30–35**):

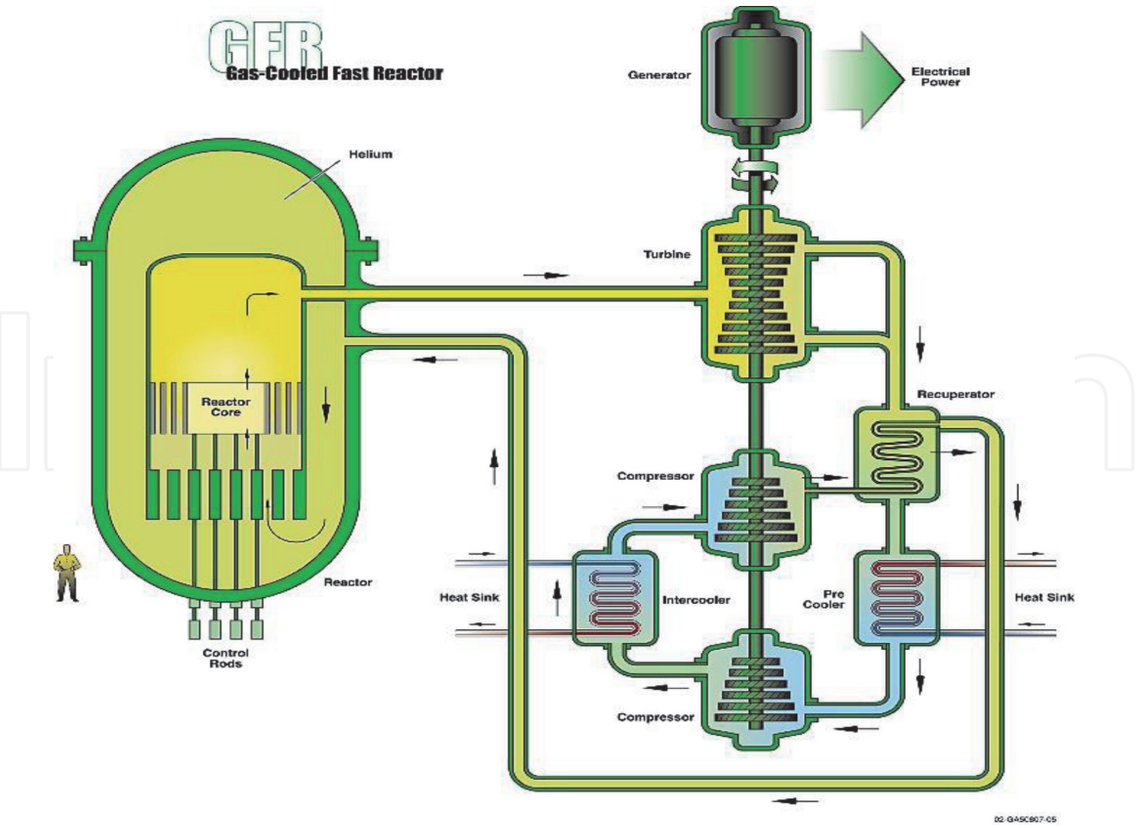

Figure 7.
Schematic of 600-MW_{th} GFR concept considered initially by GIF with direct Brayton helium cycle (Courtesy of GIF) (see also [6]).

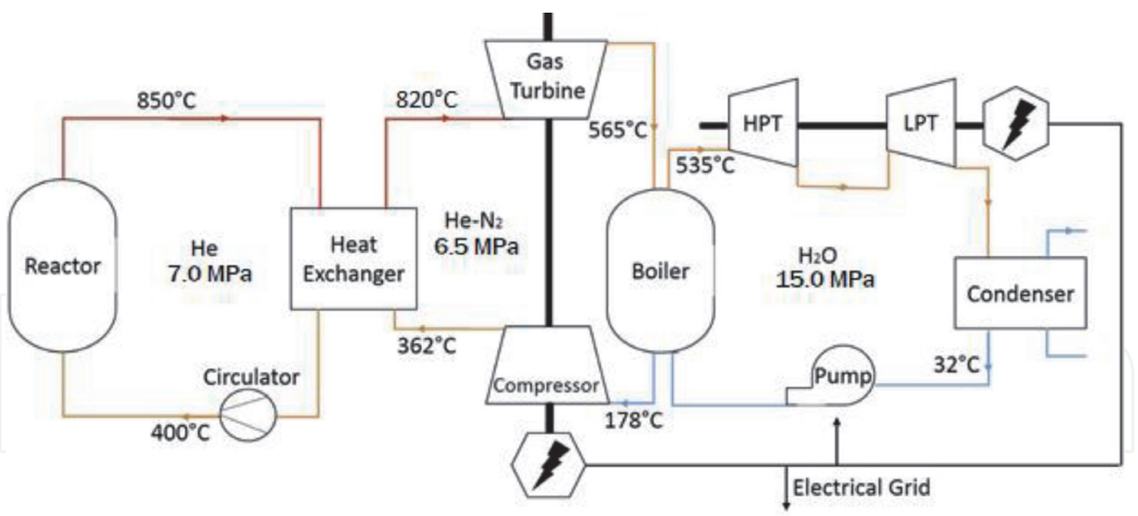

Figure 8.
Layout of 2400-MW_{th} GFR NPP with He-N_2 indirect combined power cycle (based on figure from Anzieu [23]) [18].

1. Normal heat transfer;

2. Improved heat transfer; and

3. Deteriorated heat transfer.

Also, two special phenomena (for their definitions, see Section 2, Glossary) may appear along a heated surface: (1) pseudo-boiling; and (2) pseudo-film boiling.

DOI: http://dx.doi.org/10.5772/intechopen.91474

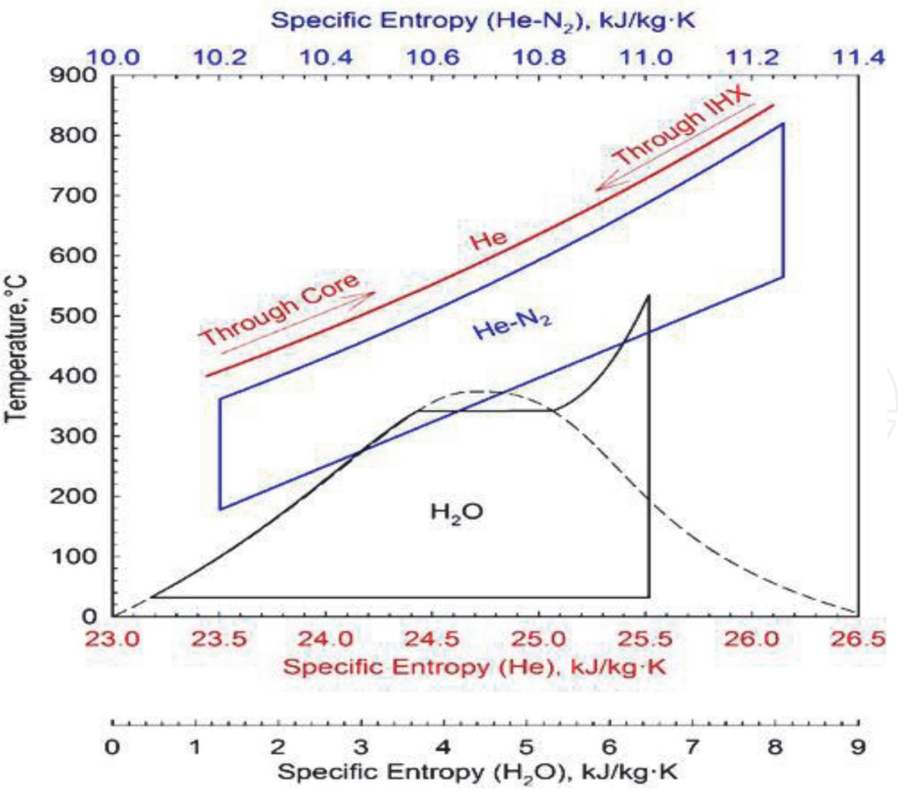

Figure 9.
T-s diagrams of 2400-MW_{th} GFR NPP combined power cycle (based on **Figure 8***) [18].*

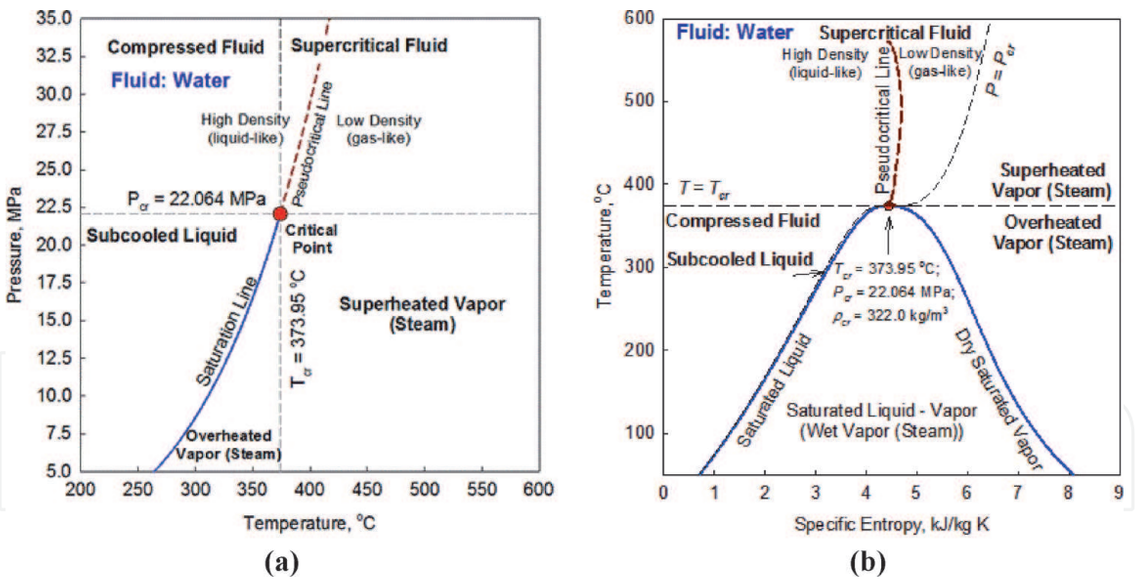

Figure 10.
Thermodynamics diagrams for water: (a) pressure-temperature and (b) temperature-specific entropy (based on NIST [25]).

These heat transfer regimes and special phenomena appear to be due to significant variations of thermophysical properties near the critical and pseudocritical points and due to operating conditions.

Therefore, the following conditions can be distinguished at critical and SCPs:

a. Wall and bulk-fluid temperatures are below a pseudocritical temperature within a part of (see **Figure 12**) or the entire heated channel (see **Figures 14a, 24a,** and **30**);

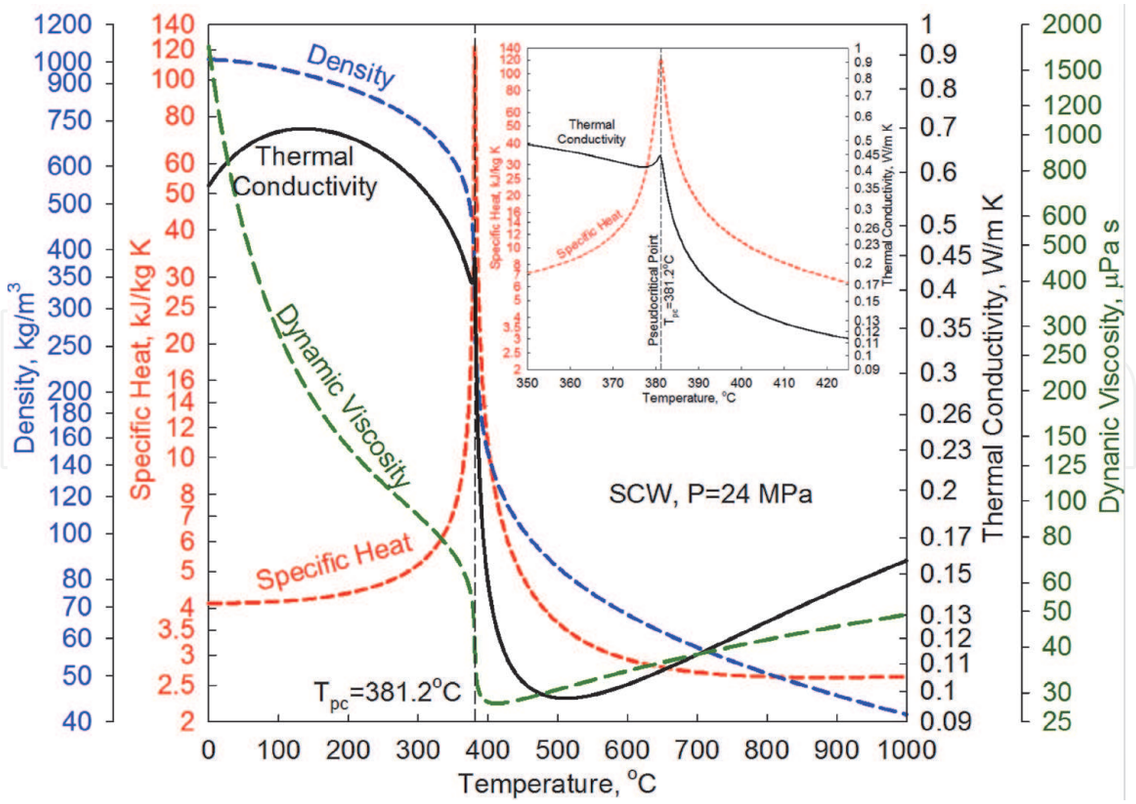

Figure 11.
Profiles of selected thermophysical properties (density, specific heat, thermal conductivity, and dynamic viscosity) vs. temperature for SCW at pressure of 24.0 MPa (based on NIST [25]).

b. Wall temperature is above, and bulk-fluid temperature is below a pseudocritical temperature within a part of (see **Figures 13a, 31, 34,** and **35**) or the entire heated channel (see **Figure 14b**);

c. Wall temperature and bulk-fluid temperature is above a pseudocritical temperature within a part of or the entire heated channel (see **Figures 12, 13a, 21, 31–35**);

d. High heat fluxes (see **Figures 13a**, **24** and **25**);

e. Entrance region (see **Figures 12, 13a, 32,** and **34**);

f. Upward and downward flows;

g. Horizontal flows; and

h. Effect of gravitational forces at lower mass fluxes; etc.

All these conditions can affect SC heat transfer.

Figure 13b shows bulk-fluid-temperature and thermophysical-properties (thermal conductivity, dynamic viscosity, specific heat, and Prandtl number) profiles along the heated length of a vertical bare circular tube (operating conditions in this figure correspond to those in **Figure 13a**).

Some researchers have suggested that variations in thermophysical properties near critical and pseudocritical points result in the maximum value of HTC. Thus, Yamagata et al. [46] found that for SCW flowing in vertical and horizontal tubes, the HTC increases significantly within the pseudocritical region (**Figure 21**). The magnitude of the peak in HTC decreases with increasing heat flux and pressure. The maximum HTC values correspond to a bulk-fluid enthalpy, which is slightly less than the pseudocritical bulk-fluid enthalpy.

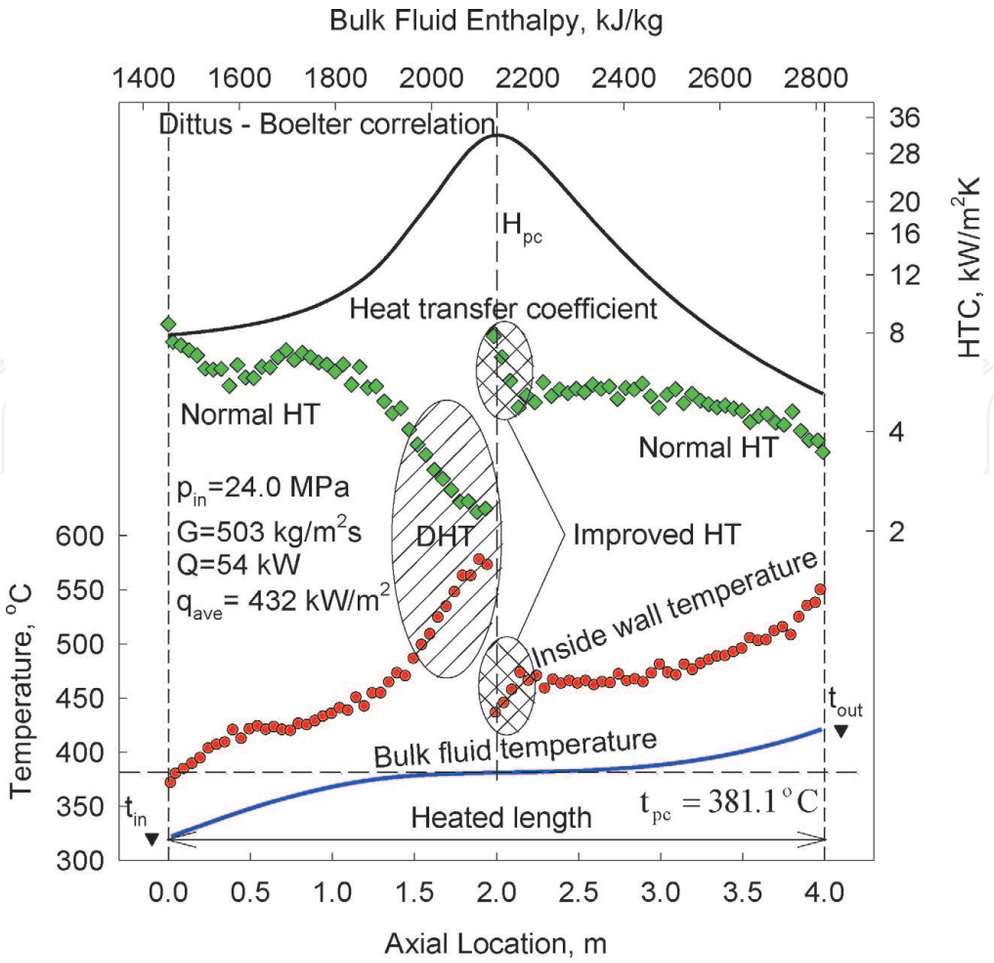

Figure 12.
Temperature and HTC profiles along heated length of vertical bare tube with upward flow of SCW (data by Kirillov et al. [26]): D = 10 mm; L_h = 4 m; q_{dht} = 316 kW/m² at G = 503 kg/m²s; points—experimental data; curves—calculated data; curve for HTC is calculated through Dittus-Boelter correlation (Eq. (1)). Profiles of density, specific heat, thermal conductivity, and dynamic viscosity vs. temperature for SCW at pressure of 24.0 MPa are shown in **Figure 11**. *Uncertainties of primary parameters are listed in* **Table 5**.

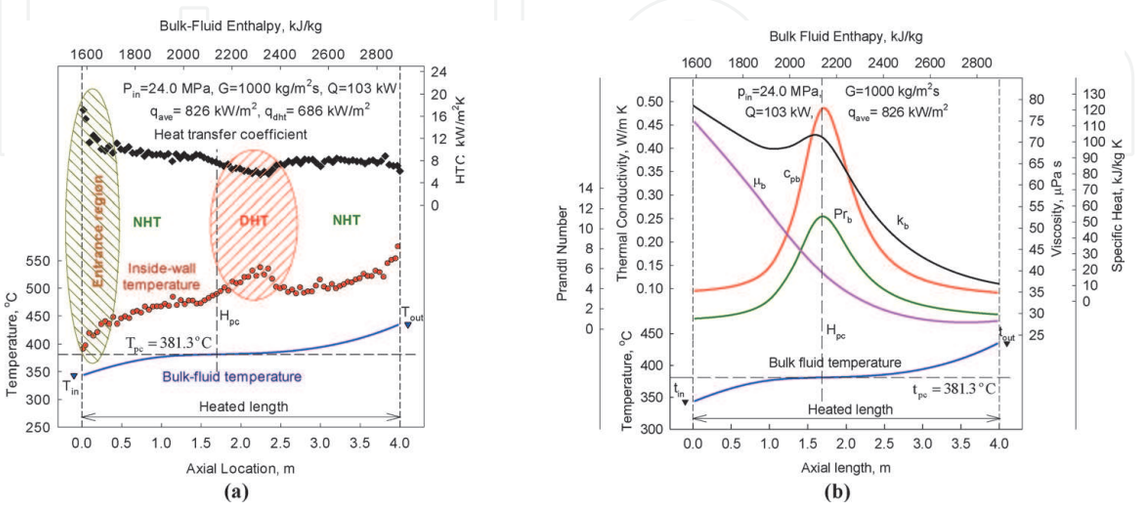

Figure 13.
(a) Temperature and HTC profiles along heated length of vertical bare tube with upward flow of SCW (data by Kirillov et al. [26]): D = 10 mm; L_h = 4 m; points—experimental data; curves—calculated data. Uncertainties of primary parameters are listed in **Table 5**; *and (b) temperature and thermophysical-properties profiles along heated length of vertical tube: operating conditions in this figure correspond to those in (a); and thermophysical properties based on bulk-fluid temperature. Profiles of density, specific heat, thermal conductivity, and dynamic viscosity vs. temperature for SCW at pressure of 24.0 MPa are shown in* **Figure 11**.

3.2 Vertical annular channel, and three- and seven-rod bundles cooled with SCW

In future SCWRs the main flow geometry will be bundles of various designs [6, 10]. Therefore, a limited number of experiments have been performed in simplified bundle simulators cooled with SCW and heated with an electrical current [10, 35–44].

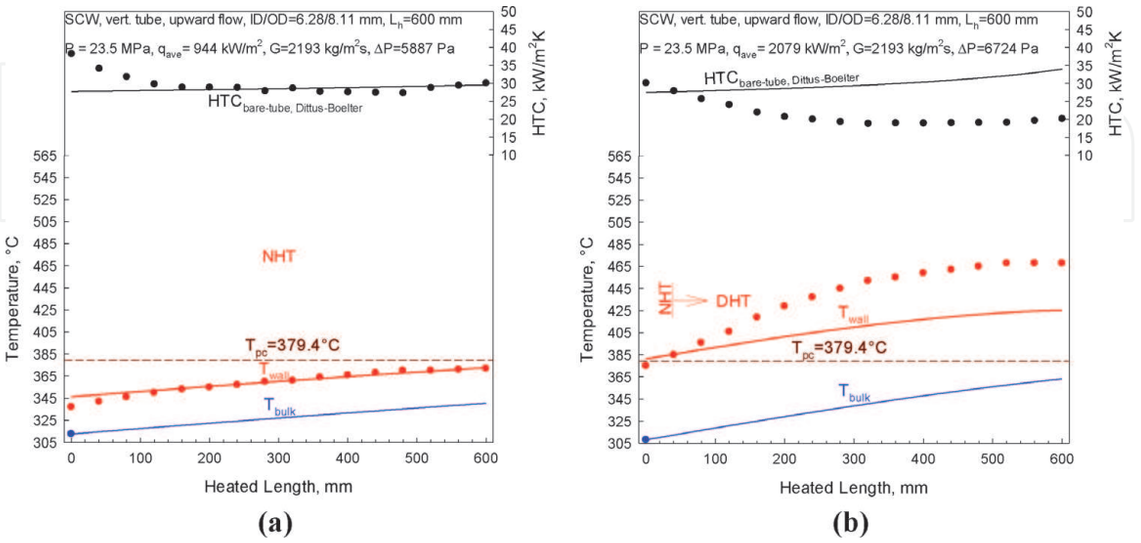

Figure 14.
Profiles of bulk-fluid and inside-wall temperatures, and HTC along heated length of vertical bare tube with upward flow of SCW at various heat fluxes: (a) q = 944 kW/m²; $T_{b\ in}$ = 313°C (entrance region can be identified within L_h = 0–150 mm) and (b) q = 2079 kW/m²; $T_{b\ in}$ = 308°C (data by Razumovskiy et al.). For both graphs, q_{dht} = 1575 kW/m² at G = 2193 kg/m²s (based on Eq. (5) [51]: P = 23.5 MPa; G = 2193 kg/m²s; and. Points—experimental data; curves—calculated data; curves for HTC and T_w are calculated through Dittus-Boelter correlation (Eq. (1)). Uncertainties of primary parameters are similar to those listed in **Table 6**.

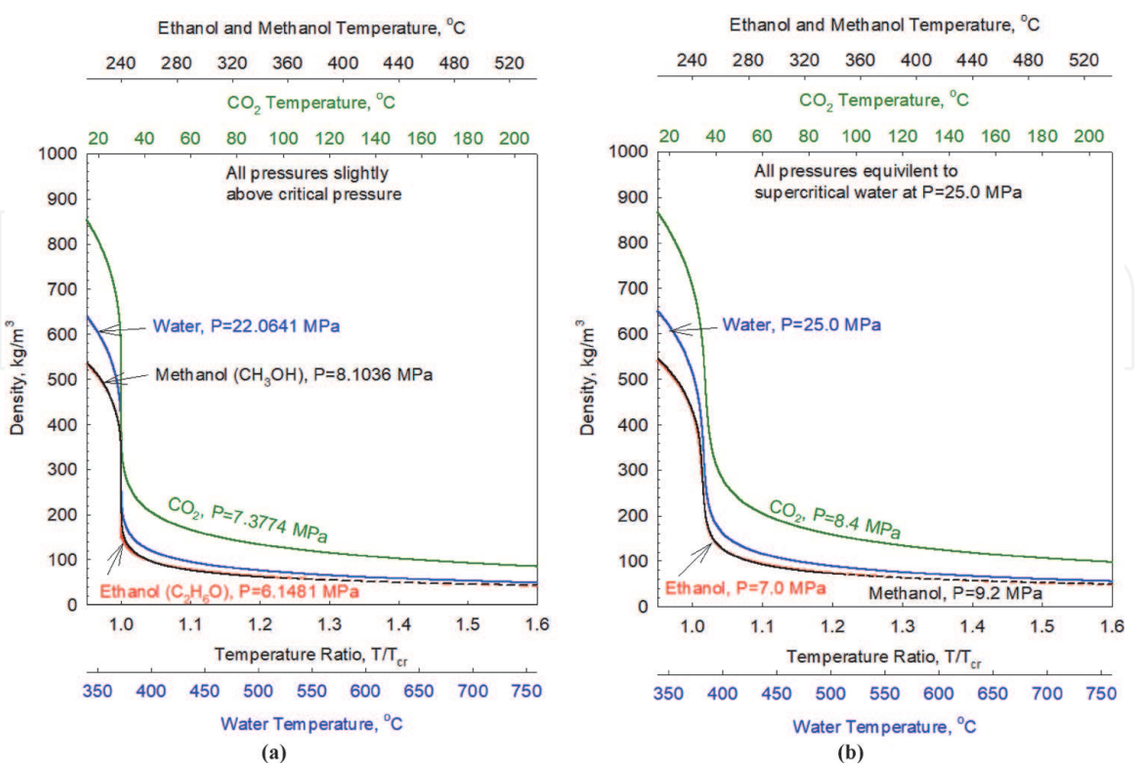

Figure 15.
Density profiles vs. reduced temperature and temperature for water, carbon dioxide, ethanol, and methanol (based on NIST [25]) (prepared by D. Mann): (a) at critical pressures; and (b) at 25 MPa for water and equivalent pressures for other SCFs (based on reduced-pressure scaling (for details, see **Table 4** *and [21])).*

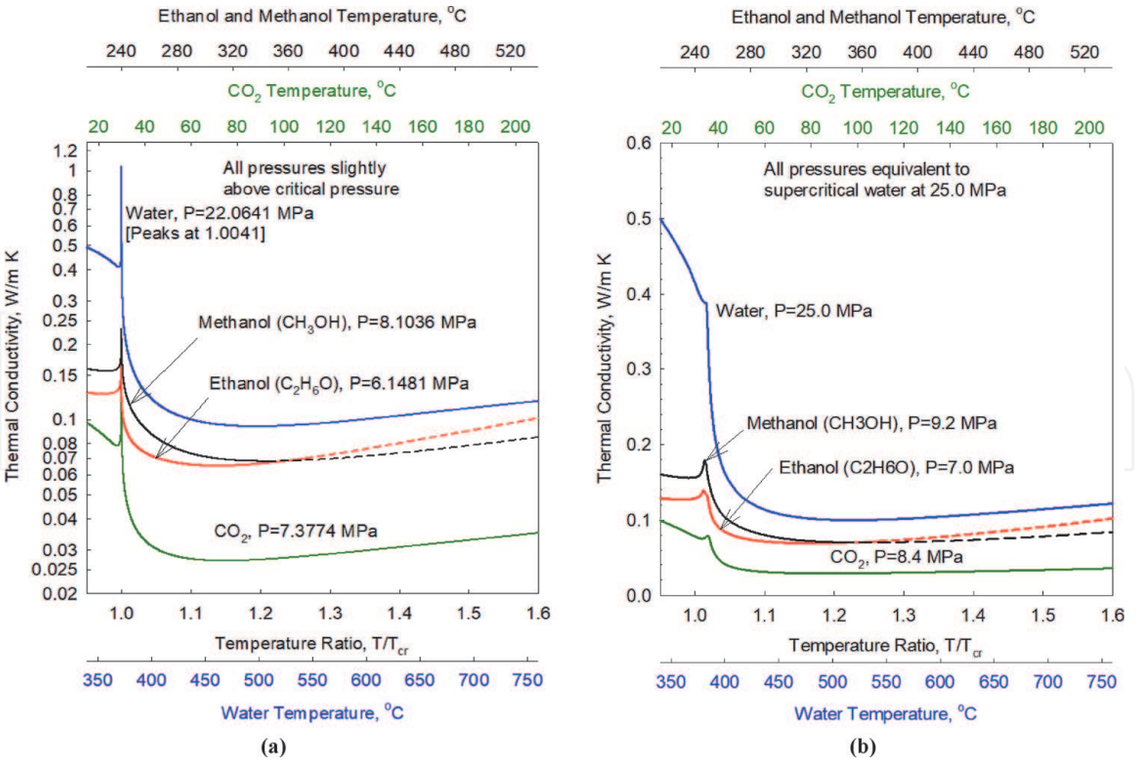

Figure 16.
Thermal-conductivity profiles vs. reduced temperature and temperature for water, carbon dioxide, ethanol, and methanol (based on NIST [25]) (prepared by D. Mann): (a) at critical pressures; and (b) at 25 MPa for water and equivalent pressures for other SCFs (based on reduced-pressure scaling (for details, see **Table 4** *and [21])).*

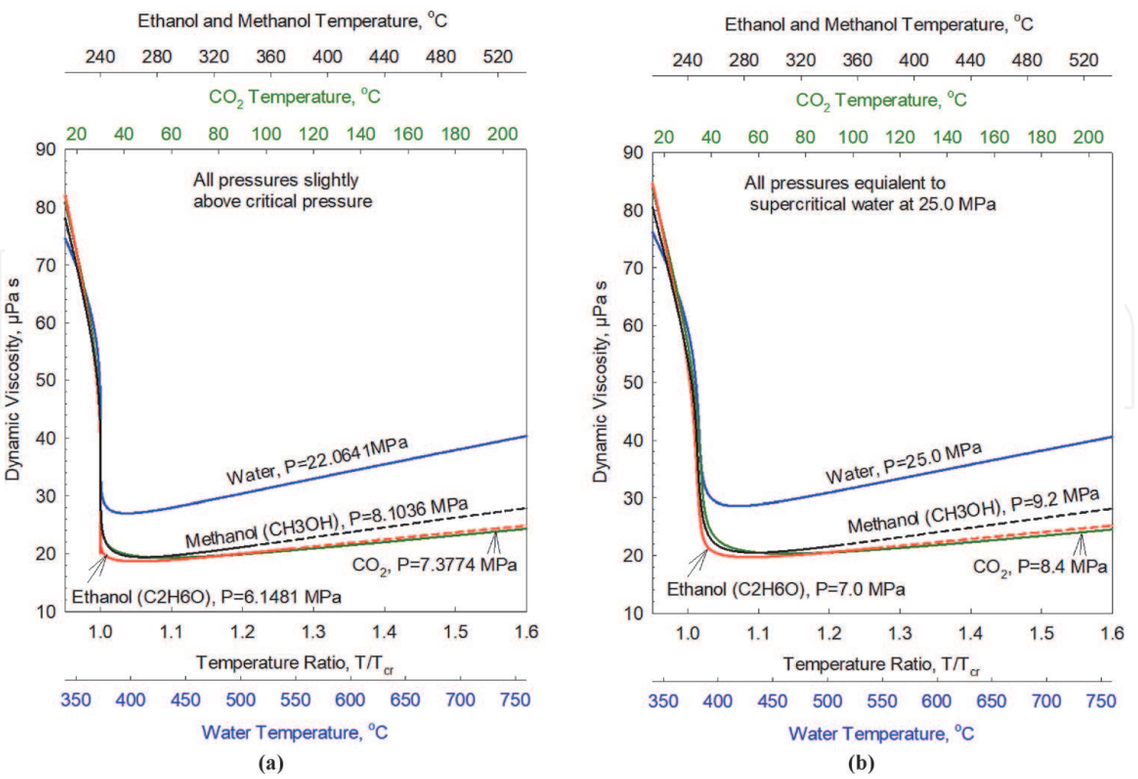

Figure 17.
Dynamic-viscosity profiles vs. reduced temperature and temperature for water, carbon dioxide, ethanol, and methanol (based on NIST [25]) (prepared by D. Mann): (a) at critical pressures; and (b) at 25 MPa for water and equivalent pressures for other SCFs (based on reduced-pressure scaling (for details, see **Table 4** *and [21])).*

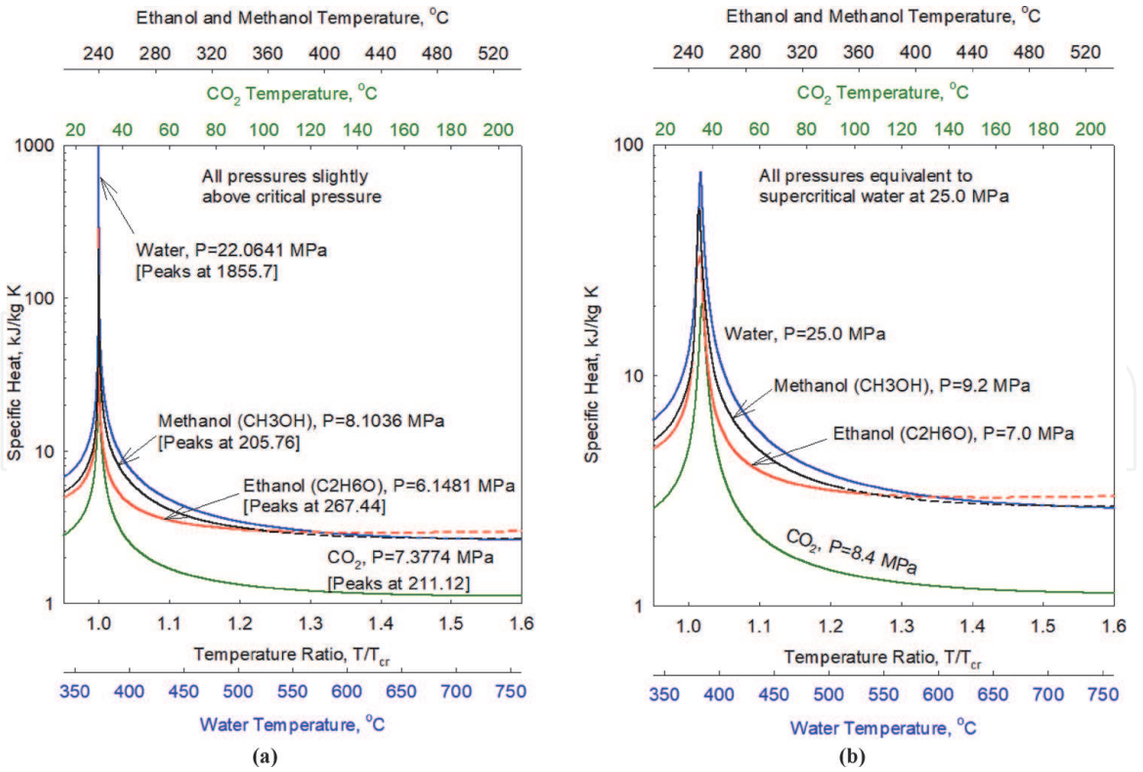

Figure 18.
Specific-heat profiles vs. reduced temperature and temperature for water, carbon dioxide, ethanol, and methanol (based on NIST [25]) (prepared by D. Mann): (a) at critical pressures; and (b) at 25 MPa for water and equivalent pressures for other SCFs (based on reduced-pressure scaling (for details, see **Table 4** *and [21])).*

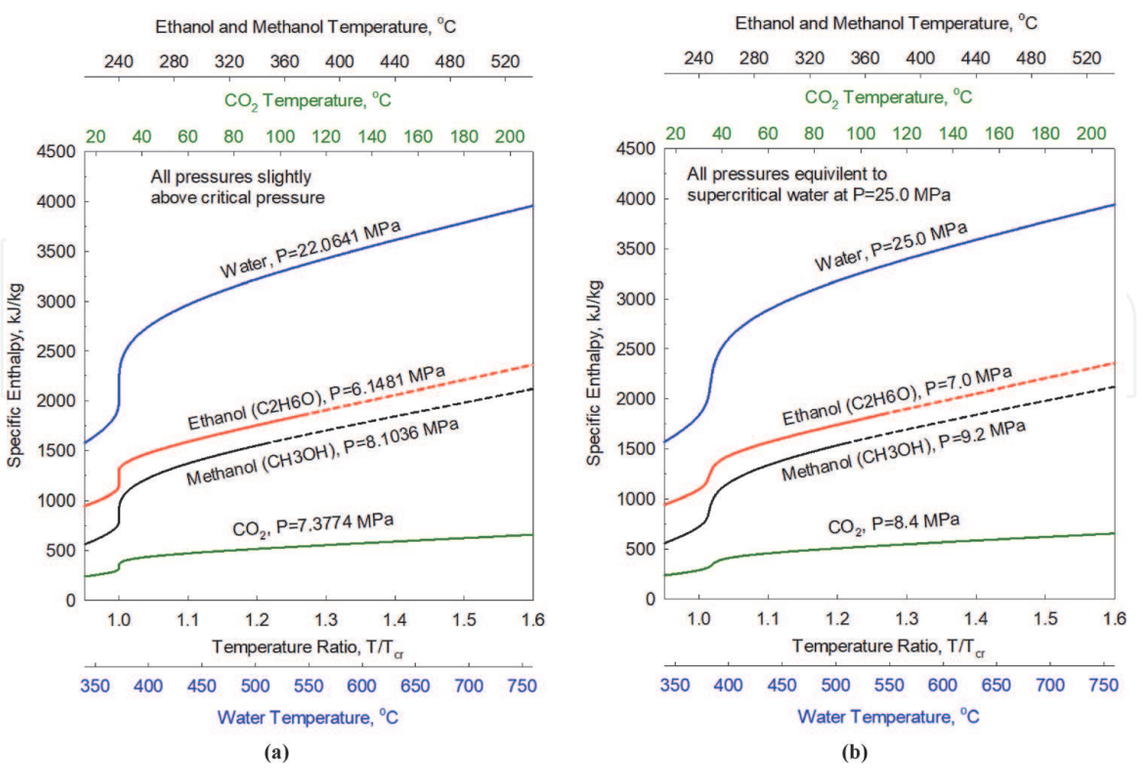

Figure 19.
Specific-enthalpy profiles vs. reduced temperature and temperature for water, carbon dioxide, ethanol, and methanol (based on NIST [25]) (prepared by D. Mann): (a) at critical pressures; and (b) at 25 MPa for water and equivalent pressures for other SCFs (based on reduced-pressure scaling (for details, see **Table 4** *and [21])).*

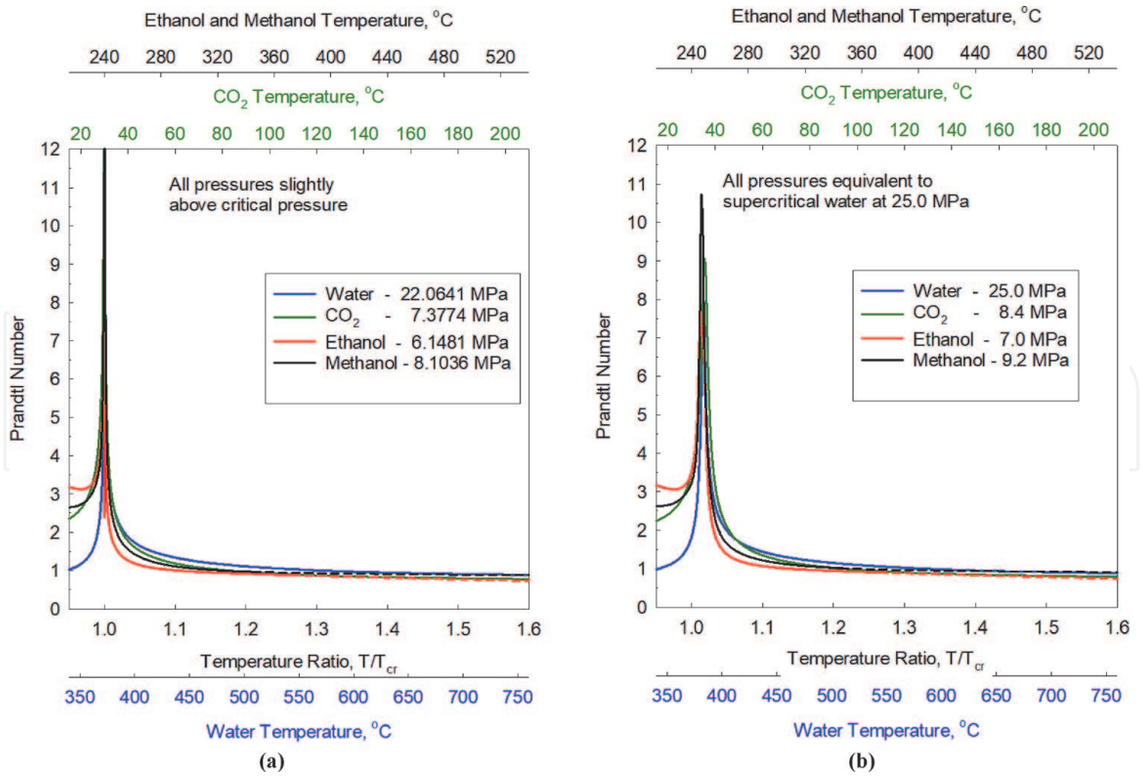

Figure 20.
Prandtl-Number profiles vs. reduced temperature and temperature for water, carbon dioxide, ethanol, and methanol (based on NIST [25]) (prepared by D. Mann): (a) at critical pressures; and (b) at 25 MPa for water and equivalent pressures for other SCFs (based on reduced-pressure scaling (for details, see **Table 4** *and [21])).*

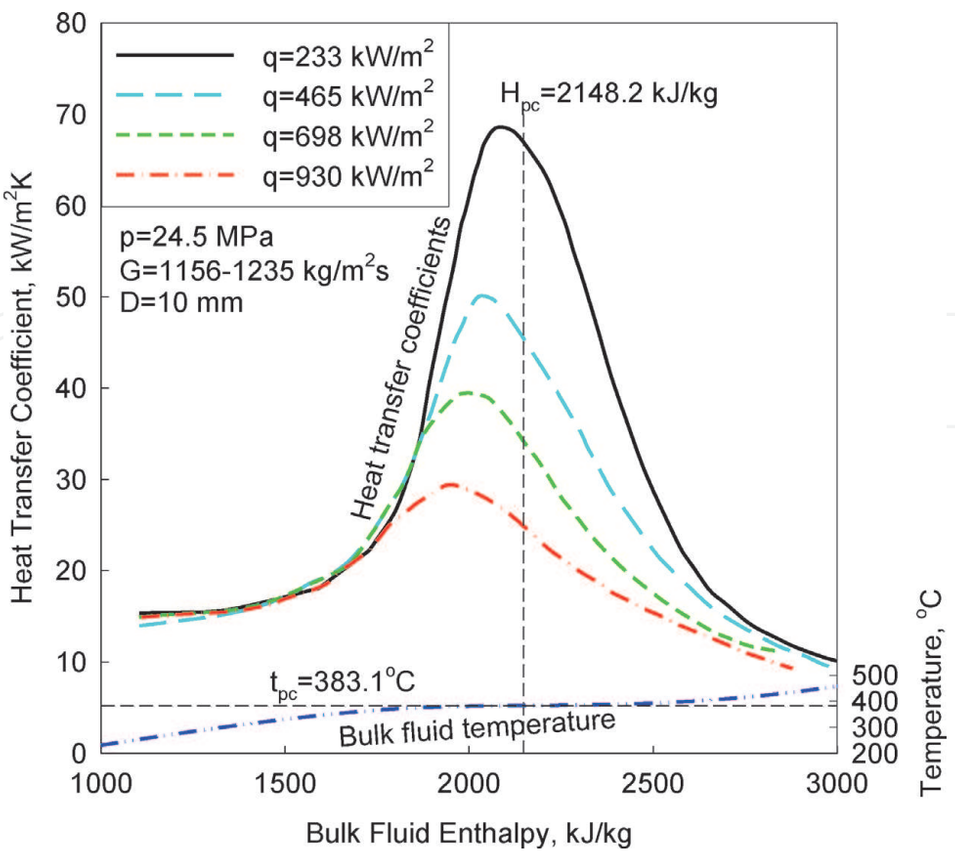

Figure 21.
Heat transfer coefficient vs. bulk-fluid enthalpy in vertical tube with upward flow of SCW at various heat fluxes (data from Yamagata et al. [46]).

An annulus or a one-rod (single-rod) bundle is the simplest bundle geometry (see **Figures 22a** and **23**), and **Figure 24** shows profiles of bulk-fluid and wall temperatures, and HTC along heated length of vertical annular channel (one-rod bundle). **Figures 22b** and **23** show three-rod-bundle flow geometry, and **Figure 25** shows profiles of bulk-fluid and wall temperatures, and HTC along heated length of vertical three-rod bundle. **Figure 26** shows seven-rod-bundle flow geometry, and **Figure 27** shows profiles of bulk-fluid and wall temperatures, and HTC along heated length of the vertical seven-rod bundle.

Analysis of data in **Figures 25b** and **27b** shows that all three HT regimes, which were noticed in bare circular tubes, are also possible in annuli and bundle flow geometries. **Figures 24** and **25** show a comparison between the HTC experimental data obtained in annulus and three-rod bundle with those calculated through the Dittus-Boelter correlation (Eq. (1)). The comparison showed that, in general, there is no significant difference between calculated HTC values and experimental ones. This finding means that in spite of the presence of rod(s) with four helical ribs in SCW flow, which can be considered as an HT enhancement surface(s), there is no significant increase in HTC. However, when q_{dht} values reached in SCW-cooled annulus and 3- and seven-rod bundles were compared to those obtained in bare tubes, it was found that q_{dht} in bare tubes were 1.6–1.8 times lower (see **Table 7**).

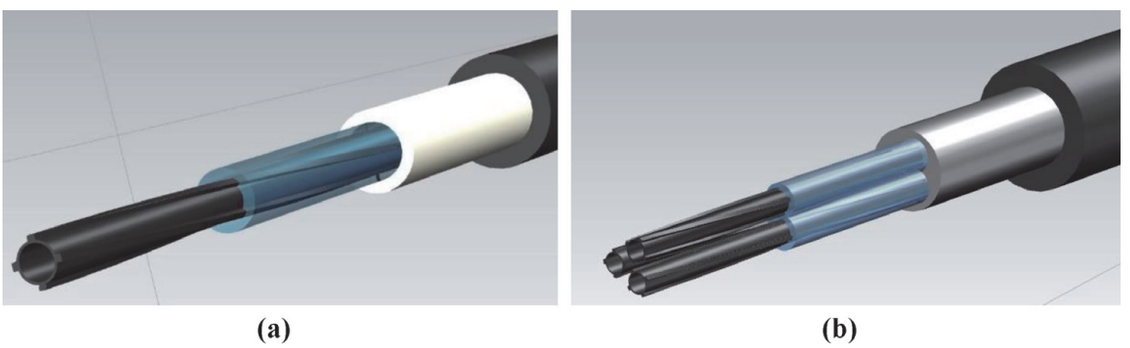

Figure 22.
3-D image of vertical annular channel (a) and three-rod bundle (b) cooled with upward flow of SCW (for other details, see **Figure 23***) [35]: heated rods equipped with four helical ribs.*

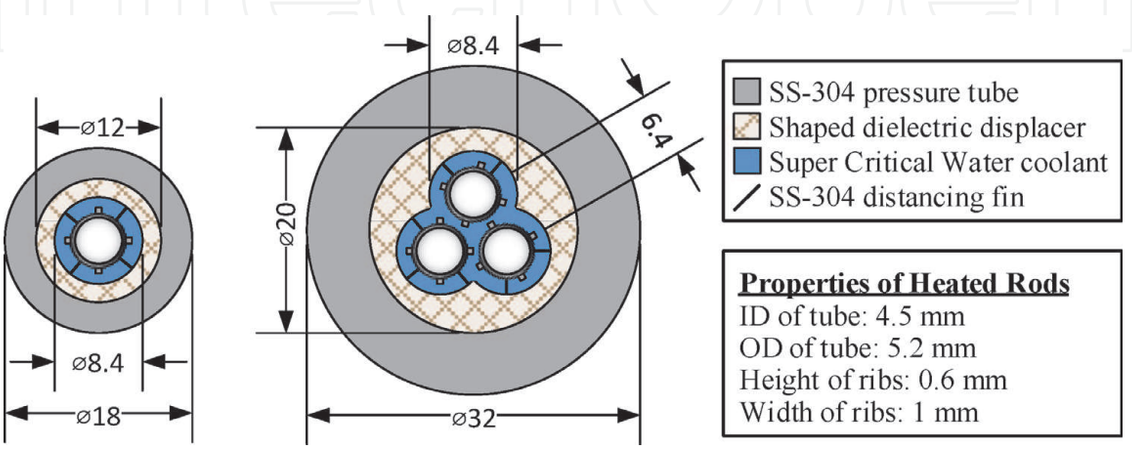

Figure 23.
Radial cross-sections of annular channel (single rod) and three-rod bundle (for other details, see **Figure 22***) [35]: heated rods equipped with four helical ribs; all dimensions in mm; and Ukrainian stainless steel has been used for heated rods, by content and other parameters, this steel is very close to those of SS-304.*

3.3 Vertical seven-rod bundle cooled with SC R-12

Figures 28 and **29** show a seven-rod bundle test section, which can be considered as a bare bundle, and **Figures 30** and **31** show profiles of bulk-fluid and wall temperatures, and HTC vs. heated length of the central rod at three circumferential locations. Analysis of **Figures 30** and **31** shows that we also have here all three HT

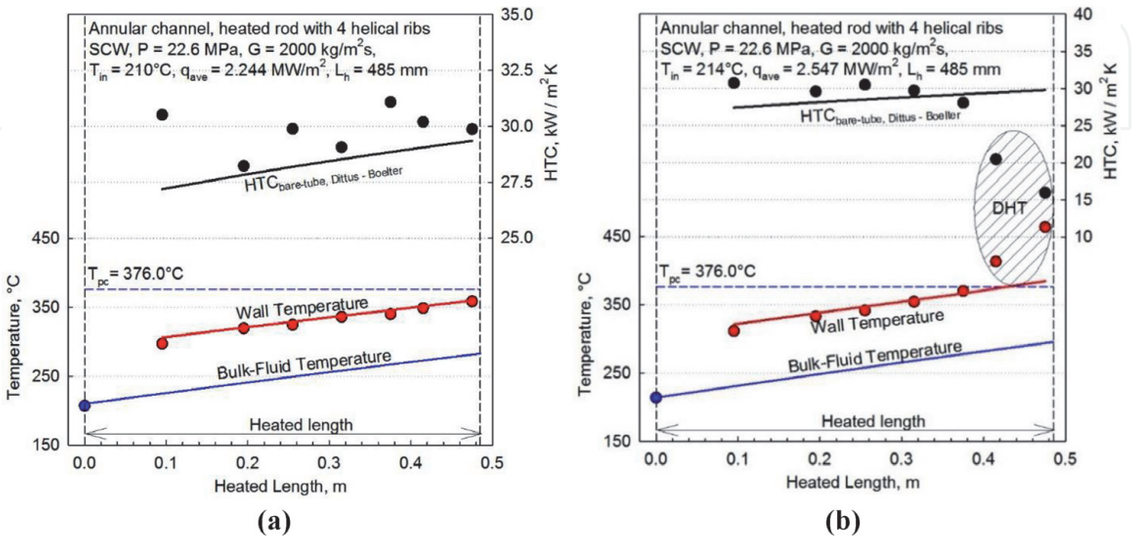

Figure 24.
Profiles of bulk-fluid and wall temperatures, and HTC along heated length of vertical annular channel (one-rod bundle; rod with four helical ribs) cooled with upward flow of SCW ([36])—P = 22.6 MPa and G = 2000 kg/m²s (bare tube q_{dht} = 1431 kW/m² (based on Eq. (5)): (a) q_{ave} = 2.244 MW/m² and T_{in} = 210°C; and (b) q_{ave} = 2.547 MW/m² and T_{in} = 214°C). For details of test section, see **Figure 23**. *Points are experimental data; curves are calculated data; curves for HTC and T_w are calculated through Dittus-Boelter correlation (Eq. (1)). Uncertainties of primary parameters are listed in* **Table 6**.

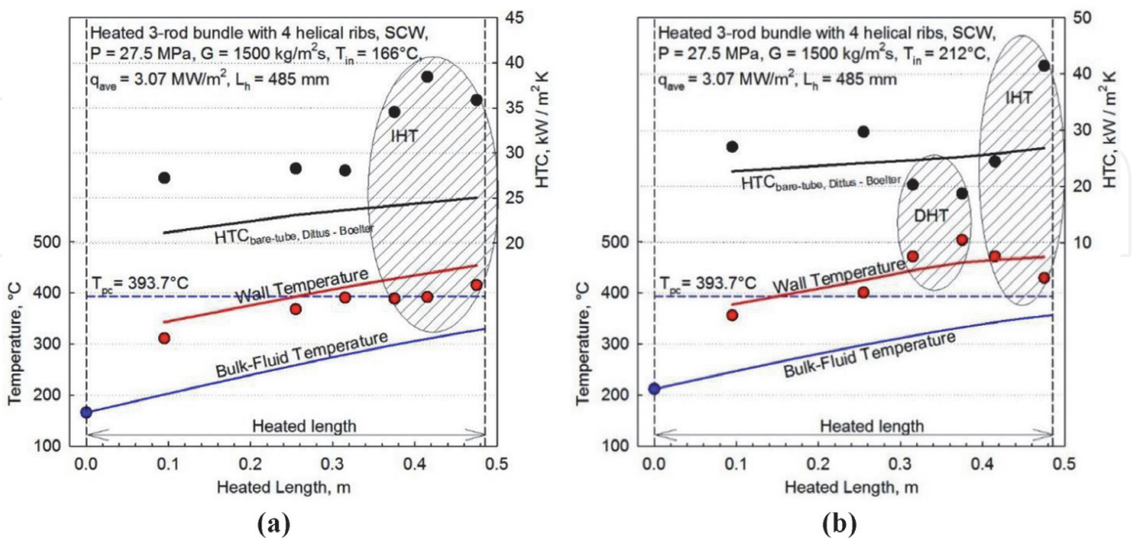

Figure 25.
Profiles of bulk-fluid and wall temperatures, and HTC along heated length of vertical annular channel (three-rod bundle; each rods with 4 helical ribs) cooled with upward flow of SCW ([36])—P = 27.5 MPa; q_{ave} = 3.07 MW/m²; G = 1500 kg/m²s (bare tube q_{dht} = 1059 kW/m² (based on Eq. (5)): (a) T_{in} = 166°C and (b) T_{in} = 212°C. Bare tube q_{dht} = 1431 kW/m² at G = 2000 kg/m²s (based on Eq. (5)); for details of test section, see **Figure 23**). *Points are experimental data; curves are calculated data; curves for HTC and T_w are calculated through Dittus-Boelter correlation (Eq. (5)). Uncertainties of primary parameters are listed in* **Table 6**.

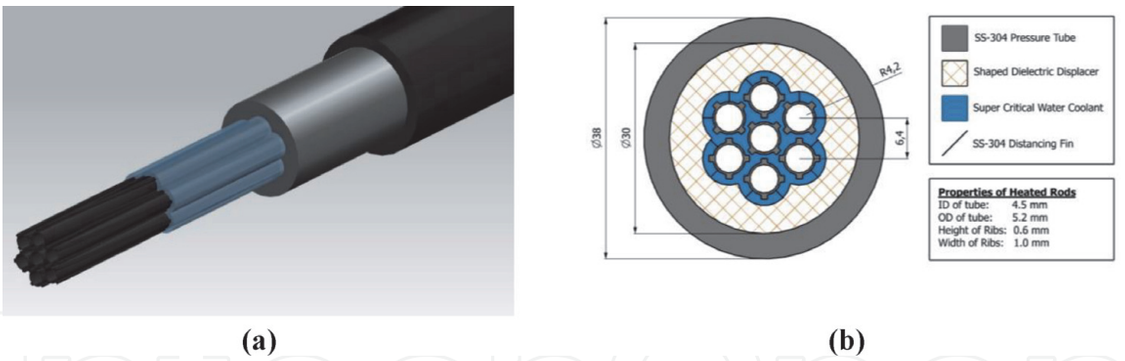

Figure 26.
3-D view (a) and cross-sectional view of vertical seven-rod bundle (b) cooled with upward flow of SCW [41, 42]: heated rods equipped with four helical ribs; all dimensions in mm; and Ukrainian stainless steel has been used for heated rods, by content and other parameters this steel is very close to those of SS-304.

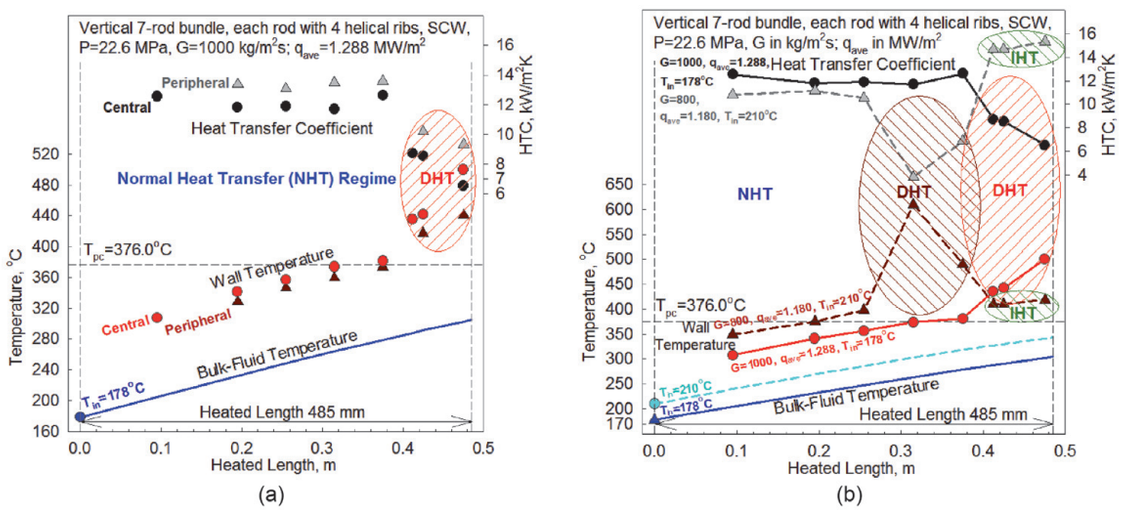

Figure 27.
Profiles of bulk-fluid and wall temperatures, and HTC vs. heated length; vertical seven-rod bundle (see **Figure 26***) cooled with upward flow of SCW [42]: P = 22.6 MPa. Uncertainties of primary parameters are listed in* **Table 6***. (a) G = 1000 kg/m²s; q_{ave} = 1.29 MW/m² (bare tube q_{dht} = 0.69 MW/m²); T_{in} = 178°C; and central and peripheral rods; (b) G = 1000; q_{ave} = 1.29 MW/m² (bare tube q_{dht} = 0.69 MW/m²); T_{in} = 178°C; and G = 800 kg/m²s; q_{ave} = 1.18 MW/m² (bare tube q_{dht} = 0.54 MW/m²); T_{in} = 210°C; and central rod.*

regimes plus sometimes quite significant differences in local HTC values and wall temperatures around the central rod circumference.

4. Practical prediction methods for forced-convection heat transfer at supercritical pressures

4.1 Supercritical water (SCW)

Unfortunately, satisfactory analytical methods for practical prediction of forced-convection heat transfer at SCPs have not yet been developed due to the difficulty in dealing with steep property variations, especially, in turbulent flows and at high heat fluxes [10, 48]. Therefore, generalized correlations based on experimental data are used for HTC calculations at SCPs.

There are numerous correlations for convective heat transfer in circular tubes at SCPs (for details, see in Pioro and Duffey [9]). However, an analysis of these correlations has shown that they are more or less accurate only within the particular

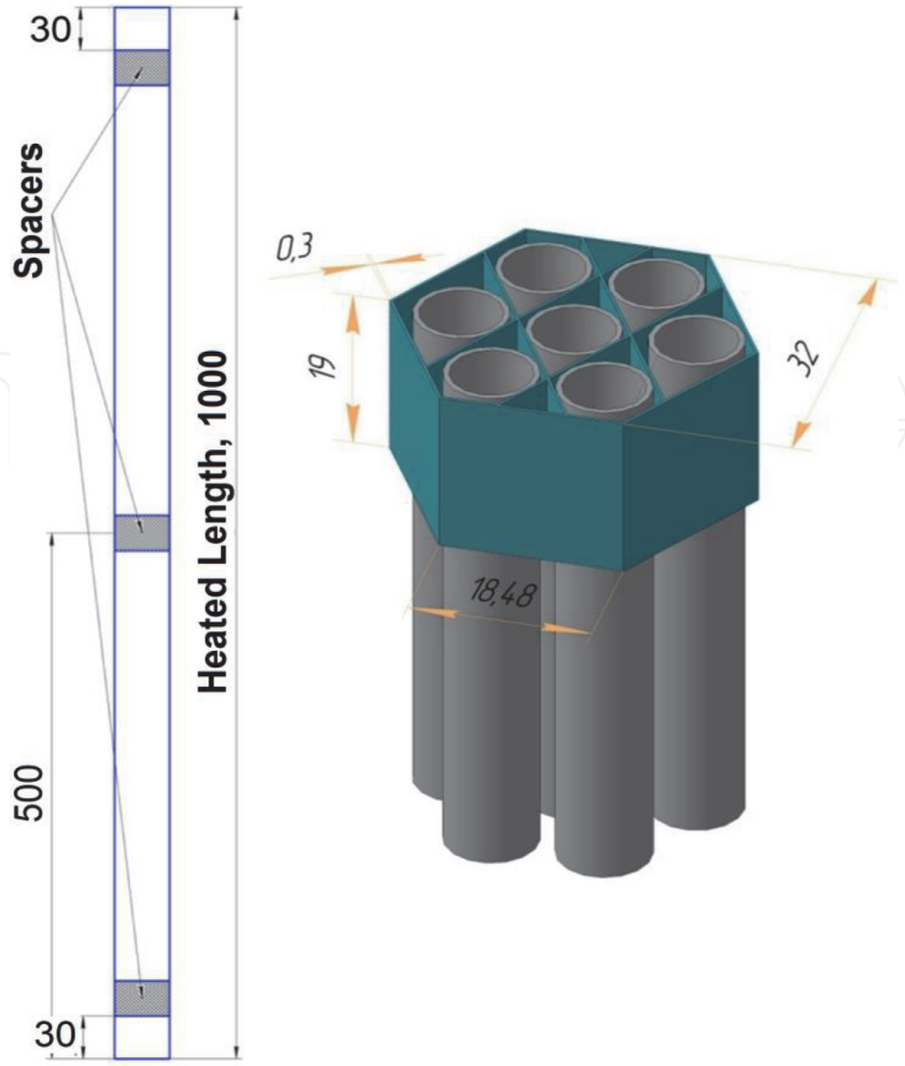

Figure 28.
Spacer grid locations and dimensions (all dimensions are in mm) [43].

dataset, which was used to derive the correlation, but show a significant deviation in predicting other experimental data. Therefore, only selected correlations are considered below.

In general, many of these correlations are based on the conventional Dittus-Boelter-type correlation (see Eq. (1)) in which the "regular" specific heat (i.e., based on bulk-fluid temperature) is replaced with the cross-sectional averaged specific heat within the range of $(T_w - T_b)$; $\left(\frac{H_w - H_b}{T_w - T_b}\right)$, J/kg K. Also, additional terms, such as: $\left(\frac{k_b}{k_w}\right)^k$; $\left(\frac{\mu_b}{\mu_w}\right)^m$; $\left(\frac{\rho_b}{\rho_w}\right)^n$; etc., can be added into correlations to account for significant variations in thermophysical properties within a cross-section due to a nonuniform temperature profile, that is, due to heat flux.

It should be noted that usually generalized correlations, which contain fluid properties at a wall temperature, require iterations to be solved, because there are two unknowns: (1) HTC and (2) the corresponding wall temperature. Therefore, the initial wall temperature value at which fluid properties will be estimated should be "guessed" to start iterations.

The most widely used heat transfer correlation at subcritical pressures for forced convection is the Dittus-Boelter [49] correlation. In 1942, McAdams [50] proposed to use the Dittus-Boelter correlation in the following form, for forced-convective heat transfer in turbulent flows:

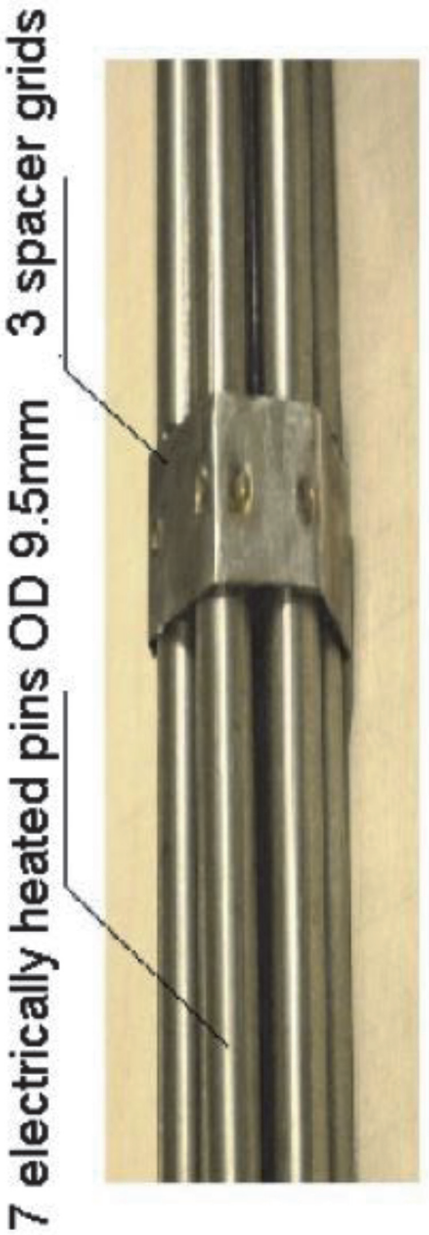

Figure 29.
Photo of central part of 7-element bundle with spacer grid [43].

$$Nu_b = 0.0243 \ Re_b^{0.8} Pr_b^{0.4} \quad (1)$$

However, it was noted that Eq. (1) might produce unrealistic results at SCPs within some flow conditions (see **Figure 12**), especially, near the critical and pseudocritical points, because it is very sensitive to properties variations.

In general, experimental HTC values show just a moderate increase within the pseudocritical region. This increase depends on mass flux and heat flux: higher heat flux—less increase. Thus, the bulk-fluid temperature might not be the best characteristic temperature at which all thermophysical properties should be evaluated. Therefore, the cross-sectional averaged Prandtl number, which accounts for thermophysical-properties variations within a cross-section due to heat flux, was proposed to be used in many SC HT correlations instead of the regular Prandtl number. Nevertheless, this classical correlation (Eq. (1)) was used extensively as a basis for various SC HT correlations [9].

The majority of empirical correlations were proposed in the 1960s–1970s [9], when experimental techniques were not at the same level (i.e., advanced level) as they are today. Also, thermophysical properties of SCW have been updated since

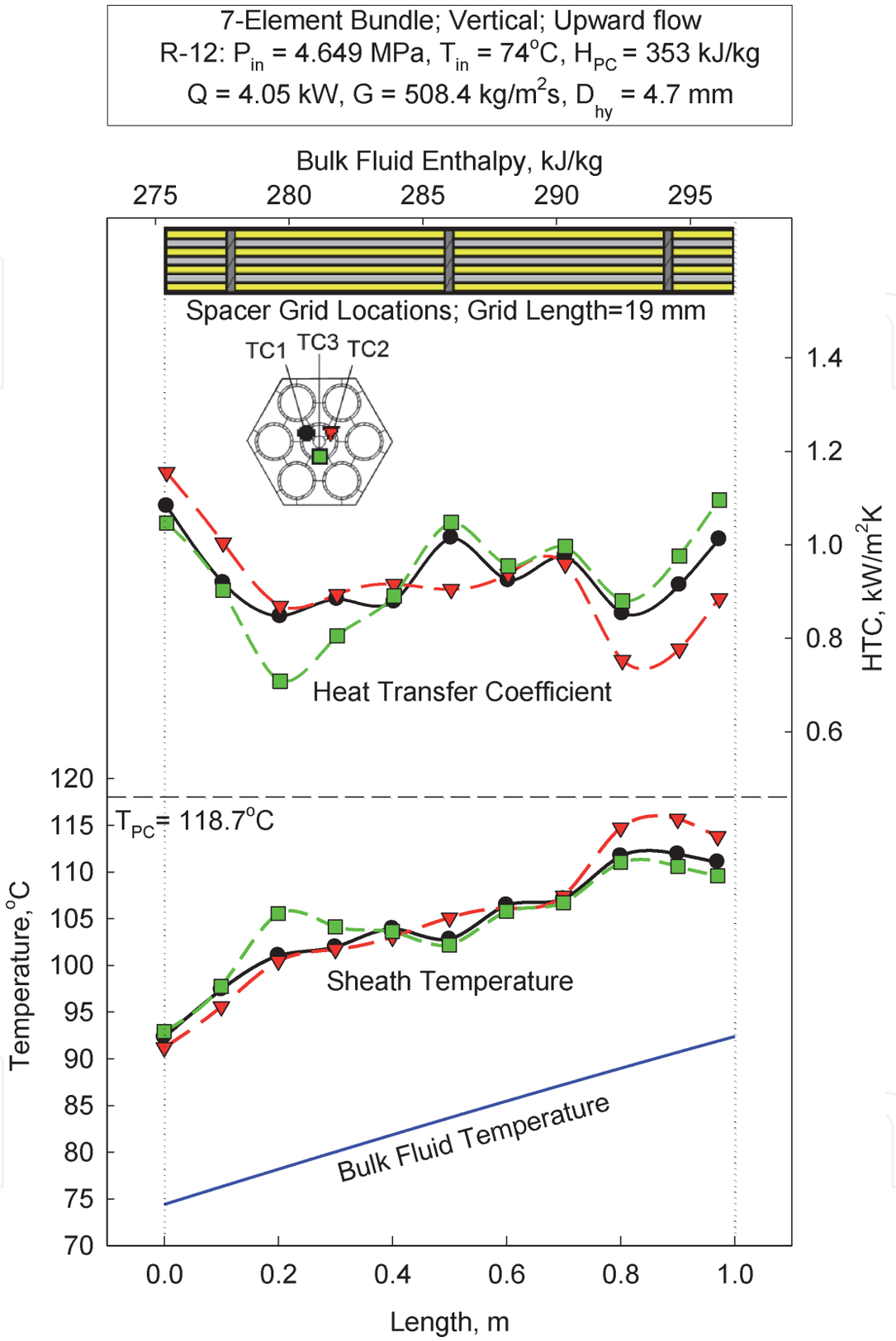

Figure 30.
Bulk-fluid and wall temperatures, and HTC profiles along heated length of vertical bare 7-element bundle (D_{hy} = 4.7 mm) cooled with upward flow of SC R-12 [43, 44]: Run 3: P_{in} = 4.65 MPa; G = 508 kg/m²s; q_{ave} = 19.4 kW/m², and T_{in} = 74°C.

that time (for example, a peak in thermal conductivity in critical and pseudocritical points within a range of pressures from 22.1 to 25 MPa for water was not officially recognized until the 1990s).

Therefore, new correlations within the SCWRs operating range, were developed and evaluated by I. Pioro with his students (mainly, by S. Mokry et al. (bulk-fluid-temperature approach) and S. Gupta et al. (wall temperature approach)) using the

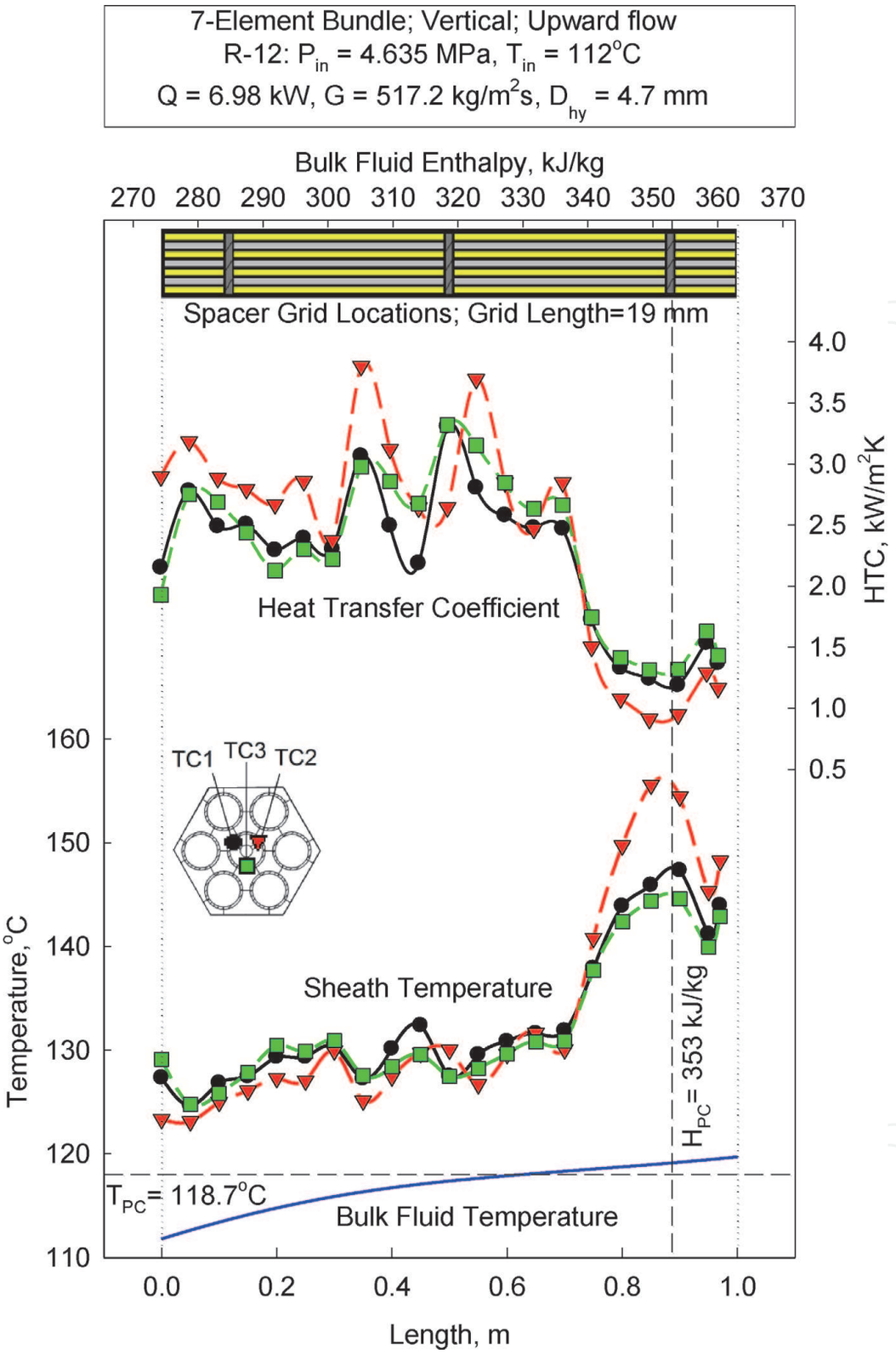

Figure 31.
Bulk-fluid and wall temperatures, and HTC profiles along heated length of vertical bare 7-element bundle (D_{hy} = 4.7 mm) cooled with upward glow of SC R-12 [43, 44]: Run 7: P_{in} = 4.64 MPa; G = 517 kg/m²s; q_{ave} = 33.4 kW/m², and T_{in} = 112°C.

best SCW dataset by P.L. Kirillov and his co-workers and adding smaller datasets by other researchers:

1. Pioro-Mokry correlation (bulk-fluid-temperature approach) [51, 52]:

$$\mathrm{Nu_b} = 0.0061 \quad \mathrm{Re_b^{0.904}\overline{Pr}_b^{0.684}}\left(\frac{\rho_w}{\rho_b}\right)^{0.564}. \tag{2}$$

The Pioro-Mokry correlation (Eq. (2)) was verified within the following operating conditions (only for NHT and IHT regimes (see **Figures 32** and **33**), but not for the DHT regime): SCW, upward flow, vertical bare circular tubes with inside diameters of 3–38 mm, pressure—22.8–29.4 MPa, mass flux—200–3000 kg/m^{2}s, and heat flux—70–1250 kW/m^2. All thermophysical properties of SCW were calculated according to NIST REFPROP software [25]. This correlation has accuracy of ±25% for HTCs and ±15 for wall temperatures (**Figure 34**). Eventually, this nondimensional correlation can be also used for other SCFs. However, its accuracy can be less or even significantly less in these cases.

2. Pioro-Gupta correlation (wall temperature approach) [53]:

$$\mathbf{Nu_w} = 0.0033\,\mathbf{Re_w^{0.941}\overline{Pr}_w^{0.764}}\left(\frac{\mu_w}{\mu_b}\right)^{0.398}\left(\frac{\rho_w}{\rho_b}\right)^{0.156} \tag{3}$$

Eq. (3) has an uncertainty of about ±25% for HTC values and about ±15% for calculated wall temperatures within the same ranges as those for Eq. (2). Also, it was decided to add an entrance effect to make this correlation even more accurate. This entrance effect was modeled by an exponentially-decreasing term as shown below:

$$\mathbf{Nu_w} = \mathbf{Nu_w}\left[1 + exp\left(-\frac{x}{24D}\right)\right]^{0.3}, \tag{4}$$

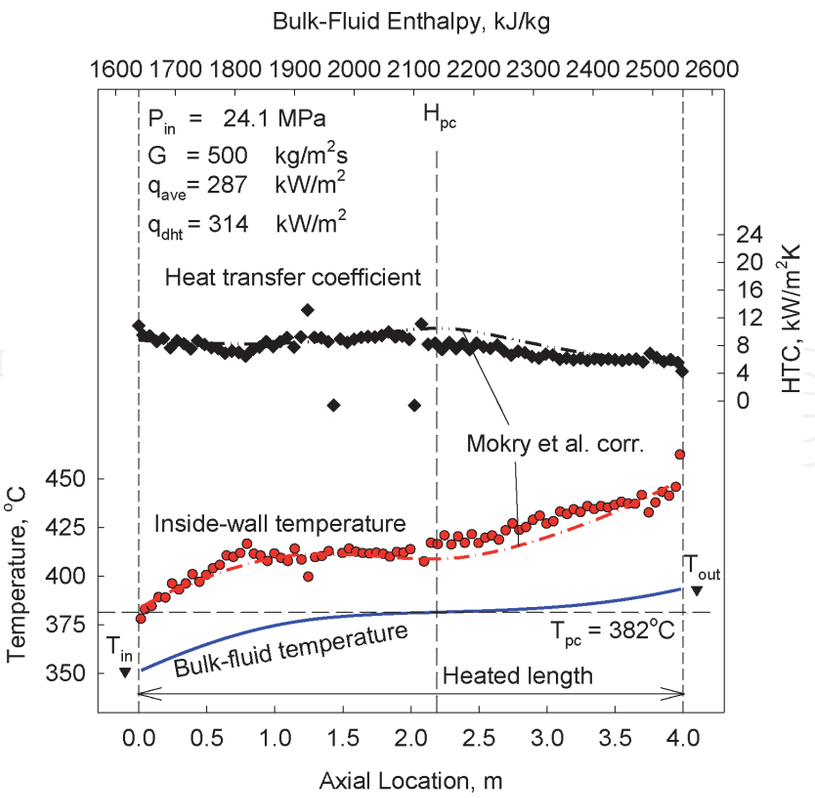

Figure 32.
Temperature and HTC profiles along 4-m circular tube (D = 10 mm) with upward flow of SCW (data by Kirillov et al. [26]) [54]: $P_{in} \approx 24$ MPa, G = 500 kg/m²s; q_{ave} = 287 kW/m²; comparison of calculated HTC values through the "proposed correlation"—Eq. (2) with experimental data within Normal Heat Transfer (NHT) regime.

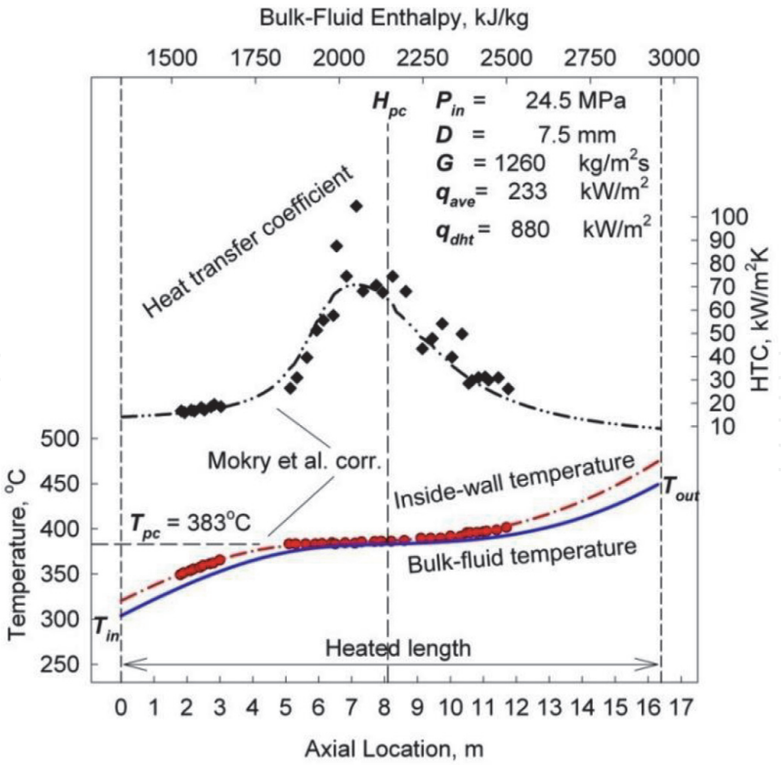

Figure 33.
Temperature and HTC profiles along circular tube (D = 7.5 mm) with upward flow of SCW (data by Yamagata et al. [46]) [54]: P_{in} = 24.5 MPa; G = 1260 kg/m²s; q_{ave} = 233 kW/m²; comparison of calculated HTC values through the "proposed correlation"—Eq. (2) with experimental data within normal and improved heat transfer (NHT and IHT) regimes.

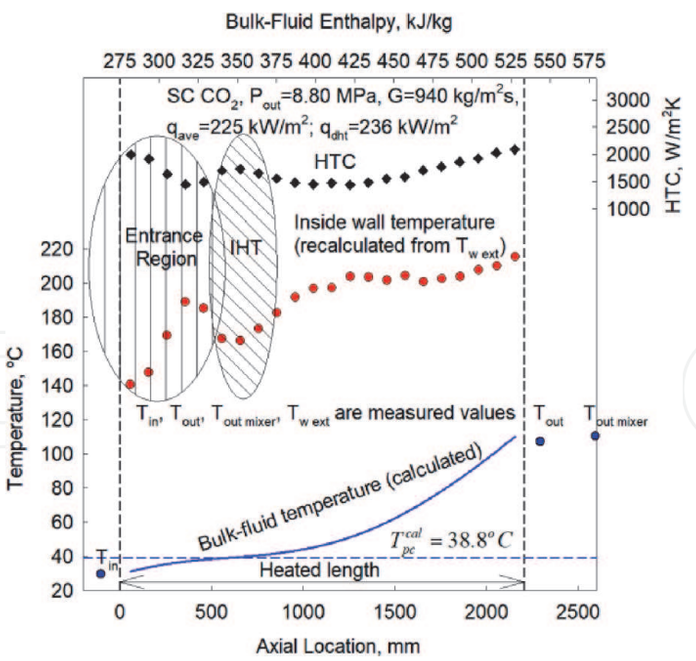

Figure 34.
Wall temperature and HTC profiles along vertical circular tube (D = 8 mm and L = 2.208 m) with upward flow of SC CO_2 (data by I. Pioro): P = 8.8 MPa; G = 940 kg/m²s; q = 225 kW/m², and T_{in} = 30°C.

where, $\mathbf{Nu}_w$ is calculated using Eq. (3). It should be noted that this HT correlation is also intended only for NHT and IHT regimes.

The following empirical correlation was proposed by I. Pioro and S. Mokry for calculating the minimum heat flux at which the DHT regime appears in vertical bare circular tubes:

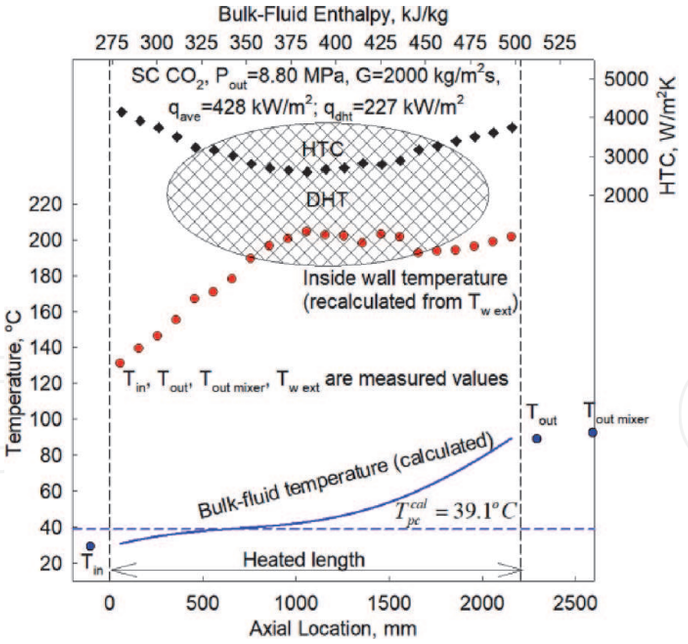

Figure 35.
Wall temperature and HTC profiles along vertical circular tube (D = 8 mm and L = 2.208 m) with upward flow of SC CO_2 (data by I. Pioro): P = 8.8 MPa; G = 2000 kg/m²s; q = 428 kW/m², and T_{in} = 29°C.

Pioro-Mokry correlation for q_{dht} [51]:

$$q_{\mathrm{dht}} = -58.97 + 0.745 \cdot G, \quad \mathrm{kW/m^2}. \tag{5}$$

Correlation (Eq. (5)) is valid within the following range of experimental parameters: SCW, upward flow, vertical bare tube with inside diameter 10 mm, pressure 24 MPa, mass flux 200–1500 kg/m²s, and bulk-fluid inlet temperature 320–350°C. Uncertainty is about ±15% for the DHT heat flux.

Wang et al. [33] have evaluated 15 q_{dht} correlations for SCW, and they have concluded that Pioro-Mokry correlation (Eq. (5)) "may be used for preliminary estimations."

A recent study was conducted by Zahlan et al. [55, 56] in order to develop a heat transfer look-up table for the critical/SCPs. An extensive literature review was conducted, which included 28 datasets and 6663 trans-critical heat transfer data (**Figure 35**). **Tables 8** and **9** list results from this study in the form of the overall-weighted average and root-mean-square (RMS) errors: (a) within three SC sub-regions; and (b) for subcritical liquid and superheated steam. Many of the correlations listed in these tables can be found in Zahlan et al. [55, 56] and Pioro and Duffey [9]. In their conclusions, Zahlan et al. [55, 56] determined that within the SC region, the latest correlation by Pioro-Mokry [51] (Eq. (2)) showed the best

Parameters	Uncertainty
Test-section power	±1.0%
Inlet pressure	±0.25%
Wall temperature	±3.0%
Mass-flow rate	±1.5%
Heat loss	≤3.0%

Table 5.
Uncertainties of primary parameters [51].

Parameters		Maximum uncertainty
Measured	Inlet pressure	±0.2%
	Bulk-fluid temperature	±3.4%
	Wall temperature	±3.2%
Calculated	Mass-flow rate	±2.3%
	Heat flux	±3.5%
	HTC	±12.7%
	Heat loss	≤3.4%

Table 6.
Maximum uncertainties of measured and calculated parameters [35–40].

No.	Test section	Operating conditions	q_{dht}, MW/m^2	Increase in q_{dht} value compared to that of bare tube
1	Bare tube	P = 24.1 MPa and G = 2000 kg/m^{2}s	1.43	1.8
2	Annulus	P = 22.6 MPa and G = 2000 kg/m^{2}s	2.55	
3	Bare tube	P = 24.1 MPa and G = 2700 kg/m^{2}s	1.95	1.6
4	Three-rod bundle	P = 22.6 MPa and G = 2700 kg/m^{2}s	3.20	
5	Bare tube	P = 24.5 MPa and G = 800 kg/m^{2}s	0.54	1.8
6	Seven-rod bundle	P = 24.5 MPa and G = 800 kg/m^{2}s	0.96	

Table 7.
Comparison of DHT values in bare-tube, annular channel (one-rod), and three-rod and seven-rod bundles [35, 42].

prediction for the data within all three sub-regions investigated (based on RMS error) (see **Table 8**). Also, the Pioro-Mokry correlation showed quite good predictions for subcritical-pressure water and superheated steam compared to other several correlations (see **Table 9**). Also, it was concluded that Pioro-Gupta correlation (Eq. (3)) was quite close by RMS errors to the Pioro-Mokry correlation.

Chen et al. [57] has also concluded that the Pioro-Mokry correlation for SCW HT "performs best" compared to other 14 correlations.

4.2 Supercritical carbon dioxide

The following correlation was proposed by S. Gupta (an MASc student of I. Pioro) [21] for SC carbon dioxide flowing inside vertical bare tubes:

$$\mathbf{Nu_w} = 0.0038\mathbf{Re_w}^{0.957}\overline{\mathbf{Pr_w}}^{-0.14}\left(\frac{\rho_w}{\rho_b}\right)^{0.84}\left(\frac{k_w}{k_b}\right)^{-0.75}\left(\frac{\mu_w}{\mu_b}\right)^{-0.22} \quad (6)$$

Uncertainties associated with this correlation are ±30% for HTC values and ± 20% for calculated wall temperatures (see **Figures 36** and **37**). Ranges of parameters for the dataset used to develop Eq. (6) are listed in **Table 10**.

Table 11 list mean and root-mean square (RMS) errors in HTC and T_w for proposed correlations using equations shown below:

It was also decided to develop the q_{dht} correlation for SC carbon dioxide based on the dataset obtained by I. Pioro in vertical bare tube with upward flow, which ranges are listed in **Table 10** [58]. Therefore, based on the identified 41 cases of

No.	Correlation	Regions					
		Liquid-like		Gas-like		Critical or pseudocritical	
		Errors, %					
		Ave.	RMS	Ave.	RMS	Ave.	RMS
1	Dittus-Boelter [49]	24	44	90	127	-	-
2	Sieder and Tate [59]	46	65	97	132	-	-
3	Bishop et al. [60]	5	28	5	20	23	31
4	Swenson et al. [61]	**1**	31	-16	21	4	23
5	Krasnoshchekov et al. [62]	18	40	-30	32	24	65
6	Hadaller and Banerjee [63]	34	53	14	24	-	-
7	Gnielinski [64]	10	36	99	139	-	-
8	Watts and Chou [65], NHT	6	30	-6	21	11	28
9	Watts and Chou [65], DHT	2	**26**	9	24	17	30
10	Griem [66]	2	28	11	28	9	35
11	Koshizuka and Oka [67]	26	47	27	54	39	83
12	Jackson [68]	15	36	15	32	30	49
13	Mokry et al. [51, 52]	-5	**26**	-9	**18**	**-1**	**17**
14	Kuang et al. [69]	-6	27	10	24	-3	26
15	Cheng et al. [70]	4	30	**2**	28	21	85
16	Gupta et al. [53]	-26	33	-12	20	**-1**	18

In bold—minimum values.

Table 8.
Overall-weighted average and RMS errors within three supercritical sub-regions (correlations are listed according to the year of publication, that is, from early ones to the latest ones) [55, 56].

No.	Correlation	Subcritical liquid		Superheated steam	
		Error, %			
		Ave.	RMS	Ave.	RMS
1	Dittus and Boelter [49]	10	23	75	127
2	Sieder and Tate [59]	28	37	84	138
3	Hadaller and Banerjee [63]	27	36	19	34
4	Gnielinski [64]	-4	**18**	80	130
5	Mokry et al. [51]	**-1**	19	**-5**	**20**

In bold—minimum values.

Table 9.
Overall average and RMS error within subcritical region [55, 56].

P, MPa	T_{in}, °C	T_{out}, °C	T_w, °C	q, kW/m^2	G, kg/m^{2}s
7.57-8.8	20-40	29-136	29-224	9.3-616.6	706-3169

Table 10.
Ranges of parameters of dataset used to develop Eq. (6).

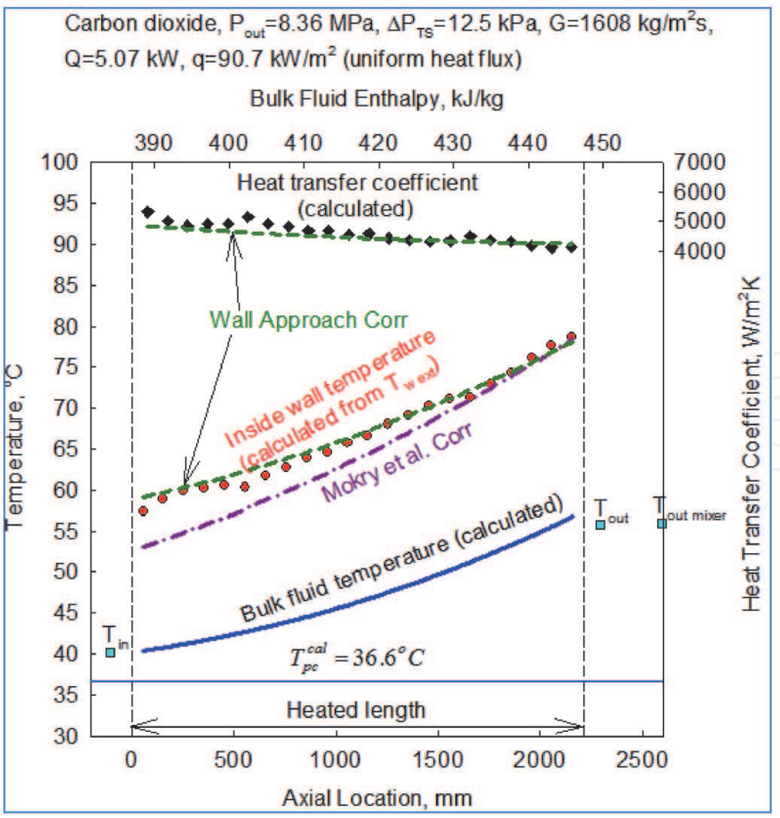

Figure 36.
HTC and T_w *variations along* L = 2.208 *m circular tube* (D = 8 *mm):* q = 90.7 *kW/m²* P = 8.4 *MPa, and* G = 1608 *kg/m²s. Wall Approach Corr. is Eq. (6) and Mokry et al. Corr. – Eq. (2).*

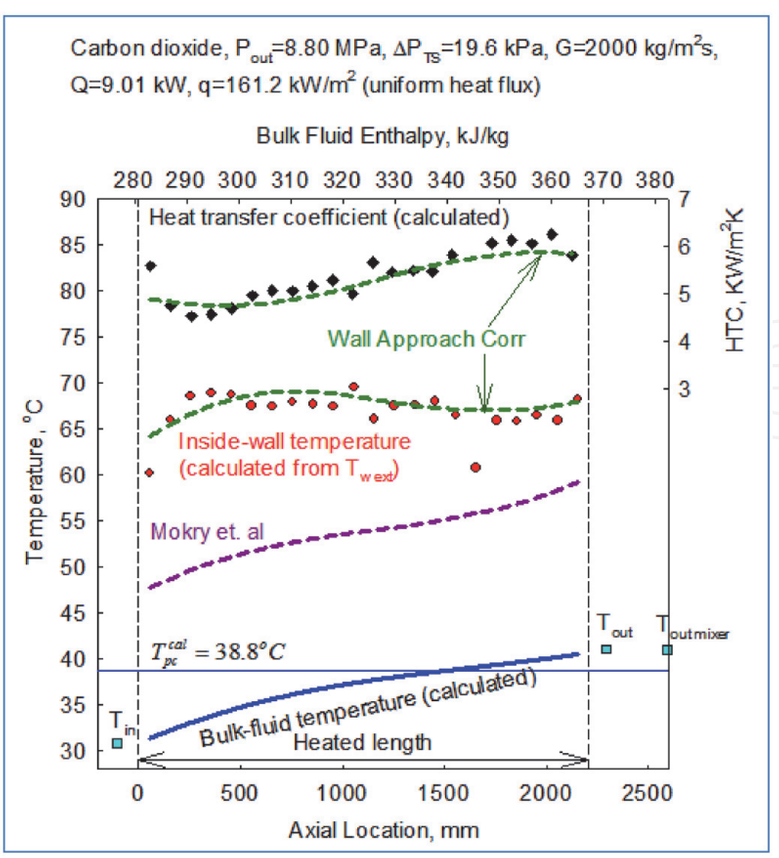

Figure 37.
HTC and T_w *variations along* L = 2.208 *m circular tube* (D = 8 *mm):* q = 161.2 *kW/m²* P = 8.8 *MPa, and* G = 2000 *kg/m²s. Wall Approach Corr. is Eq. (6) and Mokry et al. Corr. – Eq. (2).*

Errors in HTC (for the reference dataset), %		
	Mean Error	**RMS**
Proposed new correlation (T_b approach)	0.9%	22.4%
Proposed new correlation (T_{film} approach)	**0.2%**	21.7%
Proposed new correlation (T_w approach—Eq. (6))	0.8%	**20.3%**
Swenson et al. [61] correlation	89%	132%
Mokry et al. [51] correlation for SCW	68%	123%
Gupta et al. [53] correlation for SCW	78%	130%

Table 11.
Mean and RMS errors for HTC values of proposed correlations (values in bold represent minimum errors) [21].

DHT within the SC carbon dioxide dataset, the following correlation for the minimal heat flux at which deterioration occurs was proposed:

$$q_{min} = 66.81 + 0.18 \cdot G \tag{7}$$

In general, the total pressure drop for forced convection inside a channel can be calculated according to expressions listed in Pioro and Duffey [9] and Pioro et al. [71].

5. Conclusions

Supercritical fluids are used quite intensively in various industries. Therefore, understanding specifics of thermophysical properties, heat transfer, and pressure drop in various flow geometries at supercritical pressures is an important task.

In general, three major heat transfer regimes were noticed at critical and supercritical pressures in various flow geometries (vertical bare tubes, annulus, three- and seven-rod bundles) and several SCFs (SCW, SC carbon dioxide, and SC R-12): (1) normal heat transfer; (2) improved heat transfer; and (3) deteriorated heat transfer. Also, two special phenomena may appear along a heated channel: (1) pseudo-boiling; and (2) pseudo-film boiling. These heat transfer regimes and special phenomena appear to be due to significant variations of thermophysical properties near the critical and pseudocritical points and due to operating conditions.

Comparison of heat transfer-coefficient values obtained in bare circular tubes with those obtained in annulus (one-rod bundle)/three-rod bundle (rod(s) equipped with four helical ribs) shows that there are almost no differences between these values. However, the minimal heat flux at which deterioration occurs (q_{dht}) in annulus, and three- and seven-rod bundles are in 1.6–1.8 times higher compared to that recorded in bare tubes.

The current analysis of a number of well-known heat transfer correlations for supercritical fluids showed that the Dittus-Boelter correlation [49] significantly overestimates experimental HTC values within the pseudocritical range. The Bishop et al. [60] and Jackson [68] correlations tend also to deviate substantially from the experimental data within the pseudocritical range. The Swenson et al. [61] correlation provided a better fit for the experimental data than the previous three correlations within some flow conditions, but does not follow up closely the experimental data within others.

Therefore, new correlations were developed by Pioro with his students Mokry et al. [51] (bulk-fluid-temperature approach) and Gupta et al. [21] (wall temperature approach), which showed the best fit for the experimental data within a wide range of

operating conditions. These correlations have uncertainties of about ±25% for HTC values and about ±15% for calculated wall temperature. Also, based on an independent study performed by Zahlan et al. [55, 56], Pioro-Mokry correlation (given as Eq. (2)) is the best for superheated steam compared to other well-known correlations. Also, this correlation showed quite good predictions for subcritical-pressure fluids.

Acknowledgements

The author would like to express his appreciation to his former and current students, S. Clark, A. Dragunov, S. Gupta, M. Mahdi, D. Mann, S. Mokry, R. Popov, G. Richards, Eu. Saltanov, H. Sidawi, E. Tamimi, and A. Zvorykin, for their assistance in the preparation of figures and developing of correlations.

Nomenclature

A	area, m^2
c_p	specific heat at constant pressure, J/kg K
$\overline{c}_p$	averaged specific heat within the range of $(T_w - T_b)$; $\left(\frac{H_w - H_b}{T_w - T_b}\right)$, J/kg K
D	inside diameter, m
G	mass flux, kg/m^{2}s; $\left(\frac{m}{A_{fl}}\right)$
H	specific enthalpy, J/kg
h	heat transfer coefficient, W/m^{2}K
k	thermal conductivity, W/m K
L	heated length, m
m	mass-flow rate, kg/s; $(\rho \cdot V)$
P, p	pressure, Pa
Q	heat transfer rate, W
q	heat flux, W/m^2; $\left(\frac{Q}{A_h}\right)$
s	specific entropy, J/kg K
T, t	temperature, °C
T_{film}	film temperature, °C; $\left(\frac{T_w + T_b}{2}\right)$
V	volume-flow rate, m^3/s
v	specific volume, m^3/kg
x	axial coordinate, m

Greek letters

α	thermal diffusivity, m^2/s; $\left(\frac{k}{c_p \cdot \rho}\right)$
β	volumetric expansion coefficient, 1/K
Δ	difference
η	efficiency, %
μ	dynamic viscosity, Pa·s
ρ	density, kg/m^3
υ	kinematic viscosity, m^2/s; $\left(\frac{\mu}{\rho}\right)$

Non-dimensional numbers

Nu	Nusselt number; $\left(\frac{h \cdot D}{k}\right)$
Pr	Prandtl number; $\left(\frac{\mu \cdot c_p}{k}\right) = \left(\frac{\upsilon}{\alpha}\right)$

$\overline{\mathrm{Pr}}$	cross-sectional average Prandtl number within the range of $(T_w - T_b)$; $\left(\frac{\mu \cdot \bar{c}_p}{k}\right)$
Re	Reynolds number; $\left(\frac{G \cdot D}{\mu}\right)$

Subscripts or superscripts

ave.	average
b	bulk
cal	calculated
corr.	correlation
cr	critical
dht	deteriorated heat transfer
fl	flow
h	heated
hy	hydraulic-equivalent
in	inlet
max	maximum
min	minimum
out	outlet
pc	pseudocritical
sat	saturation
th	thermal
w	wall

Abbreviations and acronyms

AECL	Atomic Energy of Canada Limited
AGR	advanced gas-cooled reactor
ASME	American Society of Mechanical Engineers
Ave.	average
BN	fast sodium (reactor; in Russian abbreviations)
BWR	boiling water reactor
CHF	critical heat flux
CFD	computational fluid dynamics
corr.	correlation
CRL	Chalk River Laboratotries (AECL)
DHT	deteriorated heat transfer
GFR	Gas-cooled fast reactor
GIF	Generation-IV International Forum
HT	heat transfer
HTC	heat transfer coefficient
HTR	high-temperature reactor
HPT	high-pressure turbine
IAEA	International Atomic Energy Agency
ID	inside diameter
IHT	improved heat transfer
IHX	intermediate heat exchanger
LFR	lead-cooled fast reactor
LGR	light-water-cooled graphite-moderated reactor
LNG	liquified natural gas
LPT	low-pressure turbine

LWR	light water reactor
MSR	molten salt reactor
N/A	not applicable
NIST	National Institute of Standards and Technology (USA)
NHT	normal heat transfer
NPP	nuclear power plant
OD	outside diameter
PHWR	pressurized heavy water reactor
PWR	pressurized water reactor
REFPROP	REFerence PROPerties
RMS	root-mean square (error)
S-CO_2 (SC-CO_2)	supercritical carbon dioxide
SC	supercritical
SCF	supercritical fluid
SCP	supercritical pressure
SCW	supercritical water
SCWR	supercritical water-cooled reactor
SFR	sodium-cooled fast reactor
SS	stainless steel
TC	thermocouple
TECDOC	TEChnical DOCument
ThPP	thermal power plant
UK	United Kingdom
USA	United States of America
USSR	Union of Soviet Socialist Republics
VHTR	very high temperature reactor
WF	working fluid

Author details

Igor L. Pioro
Institute of Technology, University of Ontario, Oshawa, Ontario, Canada

*Address all correspondence to: igor.pioro@uoit.ca

References

[1] Levelt Sengers JMHL. Supercritical fluids: Their properties and applications, Chapter 1. In: Kiran E et al., editors. Supercritical Fluids. Vol. 366. Netherlands: NATO Advanced Study Institute on Supercritical Fluids—Fundamentals and Application, NATO Science Series, Series E, Applied Sciences, Kluwer Academic Publishers; 2000. pp. 1-29

[2] Schmidt E, Eckert E, Grigull V. Heat transfer by liquids near the critical state. AFF Translation, No. 527, Air Materials Command, Wright Field, Dayton, OH, USA, April; 1946

[3] Pioro LS, Pioro IL. Industrial Two-Phase Thermosyphons. New York, NY, USA: Begell House, Inc.; 1997. 288 pp

[4] Pioro I, Duffey RB, Kirillov PL, Pioro R, Zvorykin A, Machrafi R. Current status and future developments in nuclear-power industry of the world. ASME Journal of Nuclear Engineering and Radiation Science. 2019;**5**(1):27. Available from: http://nuclearenginee ring.asmedigitalcollection.asme.org/a rticle.aspx?articleID=2718229

[5] Pioro I, Kirillov P. Current status of electricity generation at nuclear power plants. In: Méndez-Vilas A, editor. Materials and Processes for Energy: Communicating Current Research and Technological Developments, Energy Book Series #1. Spain: Formatex Research Center; 2013. pp. 806-817. Available from: http://www.formatex. info/energymaterialsbook/book/ 806-817.pdf

[6] Handbook of Generation IV Nuclear Reactors. Pioro IL, editor. Duxford, UK: Elsevier, Woodhead Publishing (WP); 2016. pp. 940. Available from: https:// www.gen-4.org/gif/jcms/c_9373/pub lications

[7] Dragunov A, Saltanov E, Pioro I, Kirillov P, Duffey R. Power cycles of Generation III and III^{+} nuclear power plants. ASME Journal of Nuclear Engineering and Radiation Science. 2015;**1**(2):10

[8] Pioro I, Kirillov P. Current status of electricity generation at thermal power plants. In: Méndez-Vilas A, editor. Materials and Processes for Energy: Communicating Current Research and Technological Developments, Energy Book Series #1. Spain: Formatex research Center; 2013. pp. 796-805. Available from: http://www.formatex. info/energymaterialsbook/book/ 796-805.pdf

[9] Pioro IL, Duffey RB. Heat Transfer and Hydraulic Resistance at Supercritical Pressures in Power Engineering Applications. New York, NY, USA: ASME Press; 2007. p. 328

[10] IAEA-TECDOC-1900, 2020. Understanding and Prediction of Thermohydraulic Phenomena Relevant to Supercritical Water Cooled Reactors (SCWRs), Final Report of a Coordinated Research Project, IAEA TECDOC Series, Vienna, Austria, 544 pages. Free download from: https://www.iaea.org/ publications/13636/understanding-and-prediction-of-thermohydraulic-phenomena-relevant-to-supercritical-water-cooled-reactors-scwrs

[11] Oka Y, Koshizuka S, Ishiwatari Y, Yamaji A. Super Light Water Reactors and Super Fast Reactors. New York, NY, USA: Springer; 2010. p. 416

[12] Pioro I. The potential use of supercritical water-cooling in nuclear reactors. In: Krivit SB, Lehr JH, Kingery TB, editors. Nuclear Energy Encyclopedia: Science, Technology, and Applications. Hoboken, NJ, USA: J. Wiley & Sons; 2011. pp. 309-347

[13] Schulenberg T, Starflinger J, editors. High performance light water reactor.

In: Design and Analyses. Germany: Scientific Publishing, Karlsruher Institut fūr Technologie (KIT); 2012. p. 241

[14] Duffey R, Pioro I. Ensuring the future of nuclear power, Mechanical Engineering Magazine. ASME. 2019; **141**(11):30-35

[15] Pioro I. Current status and future developments in nuclear-power industry of the world. In: Proceedings of the international conference on climate change and the role of nuclear power, IAEA, Vienna, Austria, October 7–11, Paper No. CN275-42. 2019. p. 4

[16] Pioro I, Duffey R. Current and future nuclear-power reactors and plants, Chapter 4. In: Letcher T, editor. Managing global warming, an Interface of technology and human Issues. London, UK: Elsevier, Academic Press; 2018. p. 820

[17] Bae SJ, Ahn Y, Lee JI. Preliminary study of the supercritical CO_2 hybrid cycle for the HTGR application. In: Transactions of the Korean Nuclear Society, Spring Meeting, Jeju, Korea, May 29–30. 2014

[18] Mahdi M, Popov R, Pioro I. Research on Thermal efficiencies of various power cycles for GFRs and VHTRs. Proceedings of the 26th International Conference on Nuclear Engineering (ICONE-26), July 22–26, London, England, Paper #81618. p. 9

[19] Pioro I, Mahdi M, Popov R. Heat transfer media and their properties, Chapter 33. In: Kulacki FA, editor. Handbook of thermal science and engineering. Cham, Switzerland: Springer; 2018. pp. 1353-1446

[20] Mann D, Pioro I. Study on specifics of thermophysical properties of supercritical fluids in power engineering applications. In: Proceedings of the 23rd International Conference on Nuclear Engineering (ICONE-23), May 17–21, Chiba, Japan, Paper #1730. 2015. p. 11

[21] Gupta S, Saltanov E, Mokry SJ, Pioro I, Trevani L, McGillivray D. Developing empirical heat-transfer correlations for supercritical CO_2 flowing in vertical bare tubes. Nuclear Engineering and Design. 2013;**261**: 116-131

[22] Pioro I, Mokry S. Heat transfer to fluids at supercritical pressures, chapter. In: Belmiloudi A, editor. Heat Transfer. Theoretical Analysis, Experimental Investigations and Industrial Systems. Rijeka, Croatia: IntechOpen; 2011. pp. 481-504. Available from: http://www.intechopen.com/books/heat-transfer-theoretical-analysis-experimental-investigations-and-industrial-systems/heat-transfer-to-supercritical-fluids

[23] Anzieu P. Gas-cooled Gen-IV systems VHTR & GFR. In: Presentation for CEA Meeting, Demanova, Slovakia, February. 2010. 34 Slides

[24] Pioro I, Kirillov P. Generation IV nuclear reactors as a basis for future electricity production in the world, chapter. In: Méndez-Vilas A, editor. Materials and Processes for Energy: Communicating Current Research and Technological Developments, Energy Book Series #1. Spain: Formatex Research Center; 2013. pp. 818-830. Available from: http://www.formatex.info/energymaterialsbook/book/818-830.pdf

[25] NIST REFPROP. Reference fluid thermodynamic and transport properties. In: Lemmon EW, Bell IH, Huber ML, McLinden MO, editors. NIST Standard Reference Database 23, Version 10.0, Developers. Boulder, CO, 80305, USA: Applied Chemicals and Materials Division, National Institute of Standards and Technology (NIST); 2018

[26] Kirillov PL, Lozhkin VV, Smirnov AM. Investigation of Borders

of Deteriorated Regimes of a Channel at Supercritical Pressures (in Russian). Obninsk, Russia: State Scientific Center of Russian Federation Institute of Physics and Power Engineering by the name of A.I. Leypunskiy, FEI-2988; 2003. p. 20

[27] Generation IV International Forum (GIF). 2019. Available from: https://www.gen-4.org/gif/jcms/c_9260/public

[28] Kirillov PL, Bogoslovskaya GP. Generation IV supercritical water-cooled nuclear reactors: Realistic prospects and research program. Nuclear Energy and Technology. 2019; **5**(1):67-74

[29] Leung LKH, Nava-Dominguez A. Thermal-hydraulics program in support of Canadian SCWR concept development. ASME Journal of Nuclear Engineering and Radiation Science. 2018;**4**(1):8

[30] Peiman W, Pioro I, Gabriel K. Thermal-hydraulic and neutronic analysis of a re-entrant fuel channel design for pressure-channel supercritical water-cooled reactors. ASME Journal of Nuclear Engineering and Radiation Science. 2015;**1**(2):10

[31] Pioro IL. Current status of research on heat transfer in forced convection of fluids at supercritical pressures. Nuclear Engineering and Design. 2019;**354**:14

[32] Schatte GA, Kohlhepp A, Wieland C, Spliethoff H. Development of a new empirical correlation for the prediction of the onset of the deterioration of heat transfer to supercritical water in vertical tubes. International Journal of Heat and Mass Transfer. 2016;**102**:133-141

[33] Wang H, Leung LKH, Wang W, Bi Q. A review on recent heat transfer studies to supercritical pressure water in channels. Applied Thermal Engineering. 2018;**142**:573-596

[34] Zahlan HAM, Leung LKH, Huang Y-P, Liu G-X. Assessment of convective heat transfer correlations against an expanded database for different fluids at supercritical pressures. ASME Journal of Nuclear Engineering and Radiation Science. 2018;**4**(1):14

[35] Razumovskiy VG, Pis'mennyi EN, Sidawi K, Pioro IL, Koloskov AE. Experimental heat transfer in an annular channel and 3-rod bundle cooled with upward flow of supercritical water. ASME Journal of Nuclear Engineering and Radiation Science. 2016;**2**(1):8

[36] Razumovskiy VG, Pis'mennyi EN, Sidawi K, Pioro IL, Maevskiy EM, Koloskov AE. Specifics of heat transfer to supercritical water flowing upward in annular channel and 3-rod bundle. In: Proceedings of the 7th International Symposium on SCWR (ISSCWR-7), March 15–18, Helsinki, Finland, Paper #2095. 2015. p. 11

[37] Razumovskiy VG, Mayevskiy EM, Koloskov AE, Pis'mennyi EN, Pioro IL. Heat transfer to water at supercritical parameters in vertical tubes, annular channels, 3- and 7-rod bundles. In: Proceedings of the 21st International Conference on Nuclear Engineering (ICONE-21), July 29–August 2, Chengdu, China, Paper #16442. 2013. p. 8

[38] Razumovskiy VG, Pis'mennyy EN, Koloskov AE, Pioro IL. Heat transfer to supercritical water in vertical annular channel and 3-rod bundle. In: Proceedings of the 17th International Conference on Nuclear Engineering (ICONE-17), Brussels, Belgium, July 12–16, Paper #75212. 2009. p. 6

[39] Razumovskiy VG, Pis'menny EN, Koloskov AE, Pioro IL. Heat transfer to supercritical water in vertical 7-rod bundle. In: Proceedings of the 16th International Conference on Nuclear Engineering (ICONE-16), Orlando, FL,

USA, May 11–15, Paper #48954. 2008. p. 6

[40] Sidawi K, Pioro I, Razumovskiy VG, Pis'mennyi EN, Koloskov AE. HTC correlation applications to supercritical water flowing upward in a vertical annular channel and 3-rod bundle. In: Proceedings of the 23rd International Conference on Nuclear Engineering (ICONE-23), May 17–21, Chiba, Japan, Paper #1743. 2015. p. 11

[41] Clark S, Pioro R, Zvorykin A, Fialko NM, Pioro IL. Comparison of experimental and calculated HTC values for short vertical 7-rod bundle cooled with SCW. In: Proceedings of the 39th Annual Conference of the Canadian Nuclear Society and 43rd Annual CNS/CNA Student Conference, Ottawa, ON, Canada, June 23–26, Paper #41. 2019. p. 7

[42] Zvorykin A, Pioro R, Fialko NM, Pioro IL. Specifics of heat transfer to supercritical water in vertical 7-element bundle. In: Proceedings of the 27th International Conference on Nuclear Engineering (ICONE-27), May 19–24, Tsukuba, Ibaraki, Japan, Paper #1916. 2019. p. 10

[43] Richards G, Harvel GD, Pioro IL, Shelegov AS, Kirillov PL. Heat transfer profiles of a vertical bare, 7-element bundle cooled with supercritical freon R-12. Nuclear Engineering and Design. 2013;**264**:246-256

[44] Richards G. Study of heat transfer in a 7-element bundle cooled with the upward flow of supercritical Freon-12 [M.A.Sc. thesis]. Oshawa, ON, Canada: Faculty of Energy Systems and Nuclear Science, University of Ontario Institute of Technology; 2012. p. 177

[45] Leung LKH, Rao Y, Podila K. Assessment of computational tools in support of heat-transfer correlation development for fuel assembly of Canadian supercritical water-cooled reactor. ASME Journal of Nuclear Engineering and Radiation Science. 2016;**2**(1):9

[46] Yamagata K, Nishikawa K, Hasegawa S, et al. Forced convective heat transfer to supercritical water flowing in tubes. International Journal of Heat & Mass Transfer. 1972;**15**(12): 2575-2593

[47] Zvorykin A, Mahdi M, Popov R, Barati Far K, Pioro I. Heat transfer to supercritical water (liquid-like state) flowing in a short vertical bare tube with upward flow. In: Proceedings of the 26th International Conference on Nuclear Engineering (ICONE-26), July 22–26, London, England, Paper #81608. 2018. p. 14

[48] Farah A, Harvel G, Pioro I. Analysis of CFD code FLUENT capabilities for supercritical water heat transfer applications in vertical bare tubes. ASME Journal of Nuclear Engineering and Radiation Science. 2016;**2**(3):12

[49] Dittus FW, Boelter LMK. Heat Transfer in Automobile Radiators of the Tubular Type. Vol. 2(13). Berkeley: University of California; 1930. pp. 443-461 Publications in Engineering (or International Communications in Heat and Mass Transfer, 1985, Vol. 12, pp. 3–22)

[50] McAdams WH. Heat Transmission. 2nd ed. New York, NY, USA: McGraw-Hill; 1942. p. 459

[51] Mokry S, Pioro IL, Farah A, King K, Gupta S, Peiman W, et al. Development of supercritical water heat-transfer correlation for vertical bare tubes. Nuclear Engineering and Design. 2011; **241**:1126-1136

[52] Mokry S, Naidin M, Baig F, Gospodinov Y, Zirn U, Bakan K, et al. Conceptual thermal-design options for pressure-tube SCWRs with thermochemical co-generation of hydrogen. In: Proceedings of the 16th

International Conference On Nuclear Engineering (ICONE-16), Orlando, FL, USA, May 11–15, Paper #48313. 2008. p. 13

[53] Gupta S, Mokry S, Pioro I. Developing a heat-transfer correlation for supercritical-water flowing in vertical tubes and its application in SCWR. In: Proceedings of the 19th International Conference on Nuclear Engineering (ICONE-19), Makuhari, Japan, May 16–19, Paper #43503. 2011. p. 11

[54] Mokry S. Development of a heat-transfer correlation for supercritical water in SCWR applications [M.A.Sc. thesis]. Oshawa, ON, Canada: Faculty of Energy Systems and Nuclear Science, University of Ontario Institute of Technology; 2009. p. 190

[55] Zahlan H, Groeneveld D, Tavoularis S. Look-up table for trans-critical heat transfer. In: Proc. 2nd Canada-China Joint Workshop on Supercritical Water-Cooled Reactors (CCSC-2010), Toronto, Ontario, Canada: Canadian Nuclear Society (CNS), April 25-28. 2010

[56] Zahlan H, Groeneveld DC, Tavoularis S, Mokry S, Pioro I. Assessment of supercritical heat transfer prediction methods. In: Proceedings of the 5th International Symposium on SCWR (ISSCWR-5), Vancouver, BC, Canada, March 13–16, Paper P08. 2011. p. 20

[57] Chen W, Fang X, Xu Y, Su X. An assessment of correlations of forced convection heat transfer to water at supercritical pressure. Annals of Nuclear Energy. 2015;**76**:451-460

[58] Saltanov E, Pioro I, Mann D, Gupta S, Mokry S, Harvel G. Study on specifics of forced-convective heat transfer in supercritical carbon dioxide. ASME Journal of Nuclear Engineering and Radiation Science. 2015;**1**(1):8

[59] Sieder NM, Tate GE. Heat transfer and pressure drop of liquids in tubes. Industrial and Engineering Chemistry. 1936;**28**(12):1429-1435

[60] Bishop AA, Sandberg RO, Tong LS. Forced convection heat transfer to water at near-critical temperatures and supercritical pressures. A.I.Ch.E.-I. Chem.E. Symposium Series. 1965;**2**: 77-85

[61] Swenson HS, Carver JR, Kakarala CR. Heat transfer to supercritical water in smooth-bore tubes. Journal of Heat Transfer, Transactions of the ASME Series C. 1965;**87**(4):477-484

[62] Krasnoshchekov EA, Protopopov VS, Van F, Kuraeva IV. Experimental investigation of heat transfer for carbon dioxide in the supercritical region. In: Gazley C Jr, Hartnett JP, Ecker ERC, editors. Proceedings of the 2nd All-Soviet Union Conference on Heat and Mass Transfer, Minsk, Belarus', May, 1964, Published as Rand Report R-451-PR. Vol. 1. 1967. pp. 26-35

[63] Hadaller G, Banerjee S. Heat transfer to superheated steam in round tubes. In: AECL Report. 1969

[64] Gnielinski V. New equation for heat and mass transfer in turbulent pipe and channel flow. International Journal of Chemical Engineering. 1976;**16**(2): 359-366

[65] Watts MJ, Chou C-T. Mixed convection heat transfer to supercritical pressure water. In: Proceedings of the 7th International Heat Transfer Conference (IHTC). Germany: Munich; 1982. pp. 495-500

[66] Griem H. A new procedure for the at near-and supercritical prediction pressure of forced convection heat transfer. International Journal of Heat Mass Transfer. 1996;**3**:301-305

[67] Koshizuka S, Oka Y. Computational analysis of deterioration phenomena and thermal-hydraulic design of SCR. In: Proceedings of the 1st International Symposium on Supercritical Water-Cooled Reactor Design and Technology (SCR-2000), Paper No. 302. 2000

[68] Jackson JD. Consideration of the heat transfer properties of supercritical pressure water in connection with the cooling of advanced nuclear reactors. In: Proceedings of the 13th Pacific Basin Nuclear Conference (PBNC-13), Shenzhen City, China, October 21–25. 2002

[69] Kuang B, Zhang Y, Cheng X. A new, wide-ranged heat transfer correlation of water at supercritical pressures in vertical upward ducts. In: Proceedings of the 7th International Topical Meeting on NUclear Reactor Thermal-Hydraulics, Operations and Safety (NUTHOS-7), Seoul, Korea, October 5–9. 2008

[70] Cheng X, Yang YH, Huang SF. A simple heat transfer correlation for SC fluid flow in circular tubes. In: Proceedings of the 13th International Topical Meeting on NUclear REactor THermalhydraulics (NURETH-13), Kanazawa City, Ishikawa Prefecture, Japan, September 27–October 2. 2009

[71] Pioro I, Duffey R, Dumouchel T. Hydraulic resistance of fluids flowing in channels at supercritical pressures (survey). Nuclear Engineering and Design. 2004;**231**(2):187-197